Article

Cell Reports

FGFR1 Oncogenic Activation Reveals an Alternative Cell of Origin of SCLC in Rb1/p53 Mice

Graphical Abstract

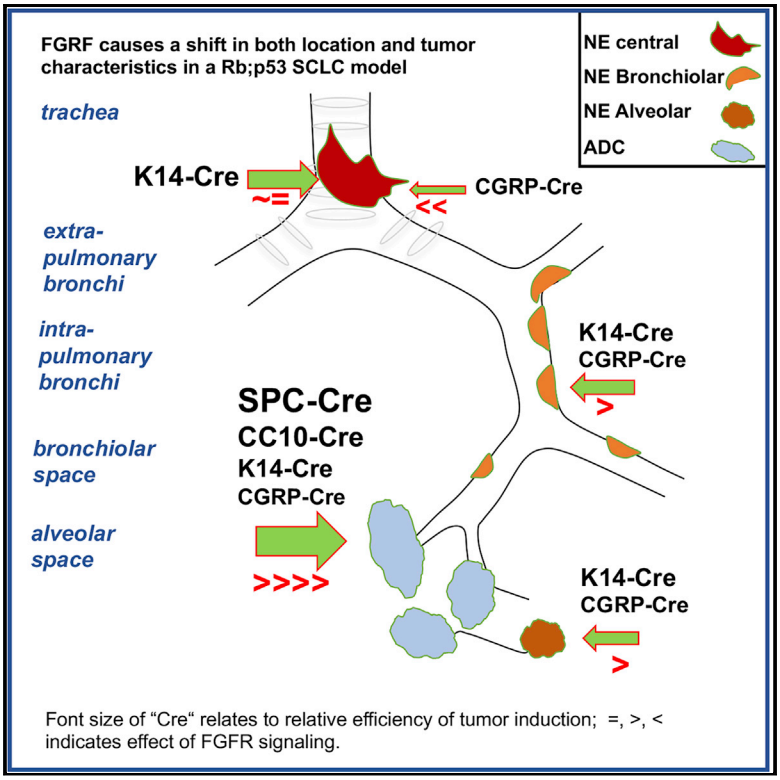

Highlights

- FGRF signaling impairs SCLC development initiated from CGRP^{POS} NE cells
- FGRF signaling promotes development of NE tumors initiated from K14^{POS} cells
- *Rb;p53*;*Fgfr1* mice develop ADCs that retain signatures of their cell of origin
- Low expression of *Fgfr1* in progressed tumors suggests a role in tumor initiation

Authors

Giustina Ferone, Ji-Ying Song, Oscar Krijgsman, ..., David J. Adams, Daniel Peeper, Anton Berns

Correspondence

a.berns@nki.nl

In Brief

Ferone et al. show that inducing FGFR signaling in lung neuroendocrine (NE) cells of *Rb;p53* mice results in impairment of SCLC and enhancement of peripheral NE lesions. The location and tumor characteristics depend on the targeted cell type. *Rb;p53*;*Fgfr1* mice also develop adenocarcinomas with the incidence depending on the targeted cell type.

Ferone et al., 2020, Cell Reports *30*, 3837–3850
March 17, 2020
https://doi.org/10.1016/j.celrep.2020.02.052

CellPress

Cell Reports
Article

FGFR1 Oncogenic Activation Reveals an Alternative Cell of Origin of SCLC in Rb1/p53 Mice

Giustina Ferone,[1] Ji-Ying Song,[2] Oscar Krijgsman,[3] Jan van der Vliet,[1] Miranda Cozijnsen,[1] Ekaterina A. Semenova,[1] David J. Adams,[4] Daniel Peeper,[3] and Anton Berns[1,5,*]

[1]Oncode Institute, Division of Molecular Genetics, the Netherlands Cancer Institute, Plesmanlaan 121, 1066 CX Amsterdam, the Netherlands
[2]Division of Molecular Oncology, the Netherlands Cancer Institute, Plesmanlaan 121, 1066 CX Amsterdam, the Netherlands
[3]Oncode Institute, Department of Experimental Animal Pathology, the Netherlands Cancer Institute, Plesmanlaan 121, 1066 CX Amsterdam, the Netherlands
[4]Wellcome Trust Sanger Institute, Wellcome Genome Campus, Cambridge CB10 1SA, UK
[5]Lead Contact
*Correspondence: a.berns@nki.nl
https://doi.org/10.1016/j.celrep.2020.02.052

SUMMARY

Fibroblast growth factor receptor 1 (FGFR1) is frequently amplified in human small-cell lung cancer (SCLC), but its contribution to SCLC and other lung tumors has remained elusive. Here, we assess the tumorigenic capacity of constitutive-active FGFR1 ($FGFR1^{K656E}$) with concomitant RB and P53 depletion in mouse lung. Our results reveal a context-dependent effect of $FGFR1^{K656E}$: it impairs SCLC development from $CGRP^{POS}$ neuroendocrine (NE) cells, which are considered the major cell of origin of SCLC, whereas it promotes SCLC and low-grade NE bronchial lesions from tracheobronchial-basal cells. Moreover, $FGFR1^{K656E}$ induces lung adenocarcinoma (LADC) from most lung cell compartments. However, its expression is not sustained in LADC originating from $CGRP^{POS}$ cells. Therefore, cell context and tumor stage should be taken into account when considering FGFR1 inhibition as a therapeutic option.

INTRODUCTION

Small-cell lung cancer (SCLC) constitutes 15% of all lung cancer cases and is the most aggressive subtype with a 5- year survival rate of 2%–8% for stage III/IV disease. Patients, frequently diagnosed with extensive disease, receive chemotherapy, often leading to a remarkable initial response. Unfortunately, patients almost invariably relapse within months with resistant disease. The standard of care first-line treatment has not changed in over 30 years, and despite ongoing efforts, no molecularly targeted drugs have been approved to date for the treatment of SCLC. However, immunotherapy with anti-PD1 antibody pembrolizumab for treating metastatic SCLC has been recently approved by the Food and Drug Administration (FDA) for patients with disease progression or after platinum-based chemotherapy and at least one other first-line treatment.

Mechanisms underlying the initial sensitivity to chemotherapy and the invariably subsequent resistance are not well understood. This highlights the importance of deeper understanding of the basic biology of SCLC, studying its initiation and progression, defining functional contribution of key drivers, and identification of the cells of origin for the tumor.

SCLC belongs to the broader class of tumors with neuroendocrine (NE) differentiation. Lung tumors with a NE phenotype can be divided in human into two major categories: (1) high-grade NE carcinomas consisting of SCLC and large cell neuroendocrine carcinoma (LCNEC) and (2) low-grade NE tumors consisting of typical and atypical carcinoids (Arrigoni et al., 1972; Mills et al., 1982).

Transformation and growth of NE tumors may be promoted by autocrine and paracrine signaling of secreted neuropeptides (Kazanjian et al., 2004; Koutsami et al., 2002). However, it is still questionable whether all NE tumors arise from the same bronchial NE cells or if cells committed to other lineages are involved (Park et al., 2011; Sutherland and Berns, 2010). It is also controversial whether the diverse NE tumors require the same molecular aberrations. So far, precursor lesions, such as tumorlets or diffuse idiopathic pulmonary neuroendocrine cell hyperplasia (DIPNECH), have been observed in man in association with carcinoids but never with other NE tumors including SCLC (Gazdar and Brambilla, 2010; Rizvi et al., 2009; Travis, 2010).

Transformation of lung cells into SCLC is promoted by the biallelic inactivation of the tumor suppressors TP53 and RB1 (George et al., 2015). In RB1-proficient tumors, overexpression of cyclin D1 may constitute an alternative mechanism, but this is relatively rare (George et al., 2015). Mice in which *Rb1* and *Trp53* are biallelically inactivated in lung cells (Meuwissen et al., 2003) recapitulate the development of human SCLC, but acquire additional lesions that are also recurrently found in human SCLC. These latter lesions were shown to accelerate tumor development and/or metastatic growth in these models. This is the case for mice that overexpress *MycL* on top of the biallelic inactivation of *Rb1* and *Trp53*, which show an earlier onset of SCLC and shortened latency of tumor development (Huijbers et al., 2014). MYCL is a transcription factor member of a family of oncogenes found amplified in ~9% of human SCLC (Calbo et al., 2011; George et al., 2015; Iwakawa et al., 2013).

The concomitant overexpression of NFIB, a transcription factor whose focal amplification was found at high frequency in $Rb1^{flox/flox};Trp53^{flox/flox}$ mice (hereafter referred to as *RP* mice), not only promoted the earlier onset of SCLC but it also enhanced

the metastatic dissemination of SCLC in mouse (Denny et al., 2016; Semenova et al., 2016).

Other mouse models based on the conditional inactivation of *Rb1* and *Trp53* in combination with either *p130* (Schaffer et al. (2010) or *Pten* (Cui et al., 2014; McFadden et al., 2014) showed the whole spectrum of NE tumors, including LCNEC and adenocarcinoma (ADC) with NE elements pointing to the substantial plasticity of lung cells.

In contrast with the genetic lesions discussed above, much less is understood about the role of fibroblast growth factor receptor 1 (*FGFR1*) amplification and therefore the activation of the mitogen-activated protein kinase (MAPK) downstream signaling pathway in SCLC. Intriguingly, in spite of its occurrence in human SCLC (Peifer et al., 2012; Voortman et al., 2010), we never found spontaneous copy number variation of *Fgfr1* in *RP* mice. Hence, it remained unclear whether its activation is beneficial to the development of SCLC, because there is evidence that the MAPK signaling pathway may play both a promoting as well as an antagonistic role.

For instance, other genetic alterations in molecules signaling through the MAPK pathway, besides *FGFR1* amplification, are rarely seen in human SCLC (George et al., 2015; Peifer et al., 2012; Rudin et al., 2012). This is the case for epidermal growth factor receptor (EGFR) amplification that has been found only in the combined subtype of SCLC with lung adenocarcinoma (LADC) (Tatematsu et al., 2008). Consistently, treatment of LADC carrying EGFR mutations with EGFR inhibitors showed a low but significant transition to SCLC (Niederst et al., 2015), suggesting that the suppression of MAPK signaling pathway might facilitate the development of SCLC. Furthermore, *in vitro* activation of this pathway resulted in impaired proliferation, growth arrest, and in some cases in loss of NE features (Calbo et al., 2011; Ravi et al., 1998, 1999; Sriuranpong et al., 2001).

However, other data suggest that the MAPK pathway can promote proliferation and survival in SCLC cell populations. As mentioned before, FGFR1 has been found focally amplified in 6% to 30% of SCLC human samples (Peifer et al., 2012; Voortman et al., 2010). Moreover, SCLC xenograft growth was impaired by inhibition of both FGFR1 and FGFR2 (Pardo et al., 2009). *In vitro* data showed that FGF2 promotes the survival of SCLC cells (Pardo et al., 2001, 2003, 2006). Furthermore, FGF2 can also contribute to the metastatic dissemination of NE tumor sub-clones (Kwon et al., 2015).

In order to unravel the contribution of FGFR1 amplification and its downstream pathway to the development of SCLC, we generated mice that conditionally overexpressed a dominant active mutant form of *Fgfr1* on top of the biallelic inactivation of *Trp53* and *Rb1*. We targeted different subpopulations of lung cells to address the potential importance of the cellular context in conjunction with these specific genetic alterations to assess how different lung cell populations respond to *Fgfr1* overexpression.

RESULTS

FGFR1^{K656E} Expression Selectively Promotes NE Bronchial Lesions, whereas It Impairs SCLC

In this study, we compared the phenotype of lung tumors in the established *RP* mouse model, which constitutes our control (Meuwissen et al., 2003), with the newly generated *Rb1*$^{flox/flox}$;*Trp53*$^{flox/flox}$;*LSL-Fgfr1*^{K656E} mouse model (hereafter *RP-Fgfr1*) (see Figure S1 and STAR Methods for description). First, we targeted all lung cell types of *RP-Fgfr1* and *RP* mice by intratracheal delivery of Ad5-CMV-Cre virus. Adenoviral delivery of Cre recombinase in pulmonary cells caused biallelic *Rb1* and *Trp53* inactivation, with concomitant induction of *Fgfr1*^{K656E} expression along with yellow fluorescent protein (YFP) from the *Col1A1* locus.

12 out of 14 *RP-Fgfr1* mice injected with Ad5-CMV-Cre showed breathing difficulties within 135 days due to the development of tumors in the nasal cavity (Table S1). Although none of the *RP-Fgfr1* mice developed SCLC within this early time-window, 58% (7 out of 12) showed neoplastic NE lesions lining the bronchi/bronchioles (BLs) (Figure 1C; Table S1), and 42% developed peripherally located NE alveolar lesions (ALs). Moreover, 33% of *RP-Fgfr1* (4 out of 12) also developed LADC.

By comparing age-matched *RP* and *RP-Fgfr1* mice, we noticed a shift in the type of CGRP-positive NE lung lesions from the typical central SCLC in 90% of *RP* mice to BLs and ALs in 80% and 70% of the *RP-Fgfr1* mice, respectively (Figures 1A–1D; Tables S1 and S2). Only 20% (2 out of 10) *RP-Fgfr1* mice developed central SCLC (Table S1). In those two mice, only a small fraction of SCLC lesions was positive to FGFR1 expression (data not shown). Furthermore, the overall tumor burden of NE lesions in *RP-Fgfr1* mice was considerably lower as compared to RP mice (Figure 1I). *RP-Fgfr1* mice that survived longer than 135 days also showed an increased penetrance of LADC whereas none of RP mice showed LADC (Tables S1 and S2).

Taken together, these data suggest that FGFR1 is disadvantageous for the development of typical SCLC, whereas it promotes BLs, ALs, and LADC when RB1 and TP53 are inactivated.

In order to study the contribution of FGFR1 to NE lesions without the confounding development of LADC, we specifically targeted NE cells of *RP-Fgfr1* and *RP* mice by intratracheal injection of Ad5-CGRP-Cre. We compared the presence of lung NE lesions in age-matched *RP-Fgfr1* and *RP* mice (170 days upon Ad5-CGRP-Cre injection). Before this time point, mice did not develop readily detectable lesions except for nasal NE tumors (Tables S3 and S4). We found that only 18% (3 out of 17) of *RP-Fgfr1* mice developed SCLC compared to 52% of *RP* mice (15 out of 29). As seen before for Ad5-CMV-Cre-injected *RP-Fgfr1* mice, in this case, only a small fraction of SCLC lesions was positive to FGFR1 expression (data not shown). The penetrance of ALs was slightly higher in *RP-Fgfr1* as compared to *RP* mice (35% versus 28%, respectively). Surprisingly, BLs were rarely found in Ad5-CGRP-Cre-injected mice as compared to Ad5-CMV-Cre-injected mice, suggesting the existence of a different cell of origin, which was not targeted by Ad5-CGRP-Cre virus. Yet, FGFR1^{K656E} expression promoted to some extent also BLs originating from CGRP^{POS} cells: 29% of *RP-Fgfr1* mice developed BLs compared to only 7% of *RP* mice. Overall, the burden of NE lesions was reduced in *RP-Fgfr1* compared to *RP* mice (Figures 1E–1H and 1J), and the type of NE lesions shifted from central to peripheral (Figures 1E–1H; Tables S3 and S4).

Unexpectedly, 41% of Ad5-CGRP-Cre treated *RP-Fgfr1* mice (7 out of 17) also developed LADC in spite of *Rb1* deletion and the NE origin of the targeted cell (Table S3). Nevertheless, the tumor burden and penetrance of LADC originating from

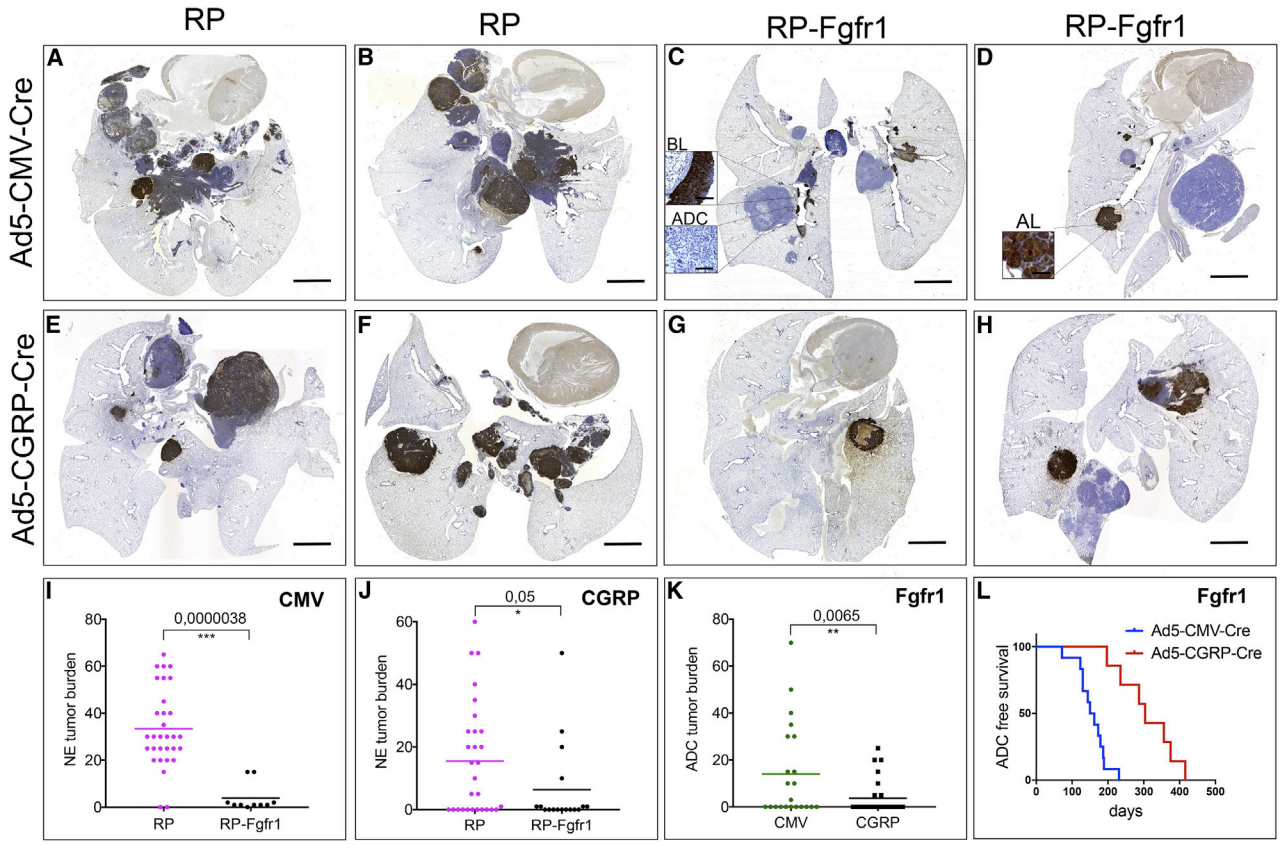

Figure 1. FGFR1 Overexpression Selectively Promotes NE Bronchial Lesions whereas It Impairs SCLC

(A–H) Scan image of CGRP staining of coronal sections of lungs from *RP* (A, B, E, and F) and *RP-Fgfr1* (C, D, G, and H) mice injected with either Ad5-CMV-Cre (A–D) or Ad5-CGRP-Cre (E–H) and collected at humane endpoint. Scale bar indicates 2 mm.

(I and J) Quantification of NE tumor burden in Ad5-CMV-Cre (CMV)-injected (I) or Ad5-CGRP-Cre (CGRP)-injected *RP* and *RP-Fgfr1* mice (J). Insets represent BL and ADC (C) and AL (D). Scale bar insets indicate 50 μm (C and D).

(K and L) Quantification of ADC tumor burden (K) and tumor-free survival curve (L) of Ad5-CMV-Cre- and Ad5-CGRP-Cre-injected *RP-Fgfr1* mice (Fgfr1).

See also Figures S1 and S4 and Tables S1, S2, S3, and S4.

CGRP^{POS} cells were much lower compared to the Ad5-CMV-Cre-induced LADC (Figure 1K; Tables S1 and S3). The onset of LADC originating from CGRP^{POS} cells occurred considerably later, allowing mice to survive longer (Figure 1L).

Taken together, our data indicate that FGFR1^{K656E} expression in RB1, TP53-deficient NE cells, imposes a shift from high grade SCLC to low grade NE tumors located mostly in the peripheral lung. Furthermore, FGFR1^{K656E} expression drives the transformation of a subset of CGRP^{POS} cells into LADC.

Our data also show that CGRP^{POS} cells are not the predominant cell of origin of BLs; nevertheless, FGFR1^{K656E} expression enables a sub-fraction of these cells to transform into BLs.

Bronchial Lesions Are Prominently Found in Ad5-CMV-Cre-Injected RP-Fgfr1 Mice and Share the Molecular Circuitry with Cisplatin-Resistant Alveolar Lesions

We compared the number of mice with BLs (penetrance) as well as the number of BLs per mouse (Figures 2A and 2B; Tables S1, S2, S3, and S4) in the different cohorts of mice and found that both were higher in *RP-Fgfr1* as compared to *RP* mice. This difference was particularly pronounced when mice were injected with Ad5-CMV-Cre and to a lesser extent with Ad5-CGRP-Cre (Figures 2A and 2B). In contrast, FGFR1^{K656E} expression had little or no impact on the number of ALs per mouse (Figures 2C and 2D), although the penetrance was slightly increased in both Ad5-CGRP-Cre- and Ad5-CMV-Cre-injected *RP-Fgfr1* mice (Tables S1, S2, S3, and S4).

Independently of the genotype, BLs expressed a high level of CGRP and CDH1 (Figures 2E and 2F and data not shown). BLs in *RP-Fgfr1* mice expressed FGFR1^{K656E} in patches along with YFP, as visualized by antibodies against GFP (Figures 2G and 2H).

To exclude that the sporadic expression of FGFR1^{K656E} in some BLs was due to partial recombination of *Fgfr1* allele, we isolated genomic DNA from FGFR1^{POS} lesions such as LADC derived from Ad5-CMV-Cre-injected mice and from FGFR1^{NEG} NE lesions (Figure 2I). We used SCLC isolated from *RP* mice as negative control of *Fgfr1*^{K656E} ectopic allele recombination. PCR analysis (Figure 2J) showed that both NE and LADC lesions with very different levels of FGFR1 protein expression had recombined the ectopic *Fgfr1*^{K656E} allele. This result indicates that the transgenic *Fgfr1*^{K656E} allele recombination is very

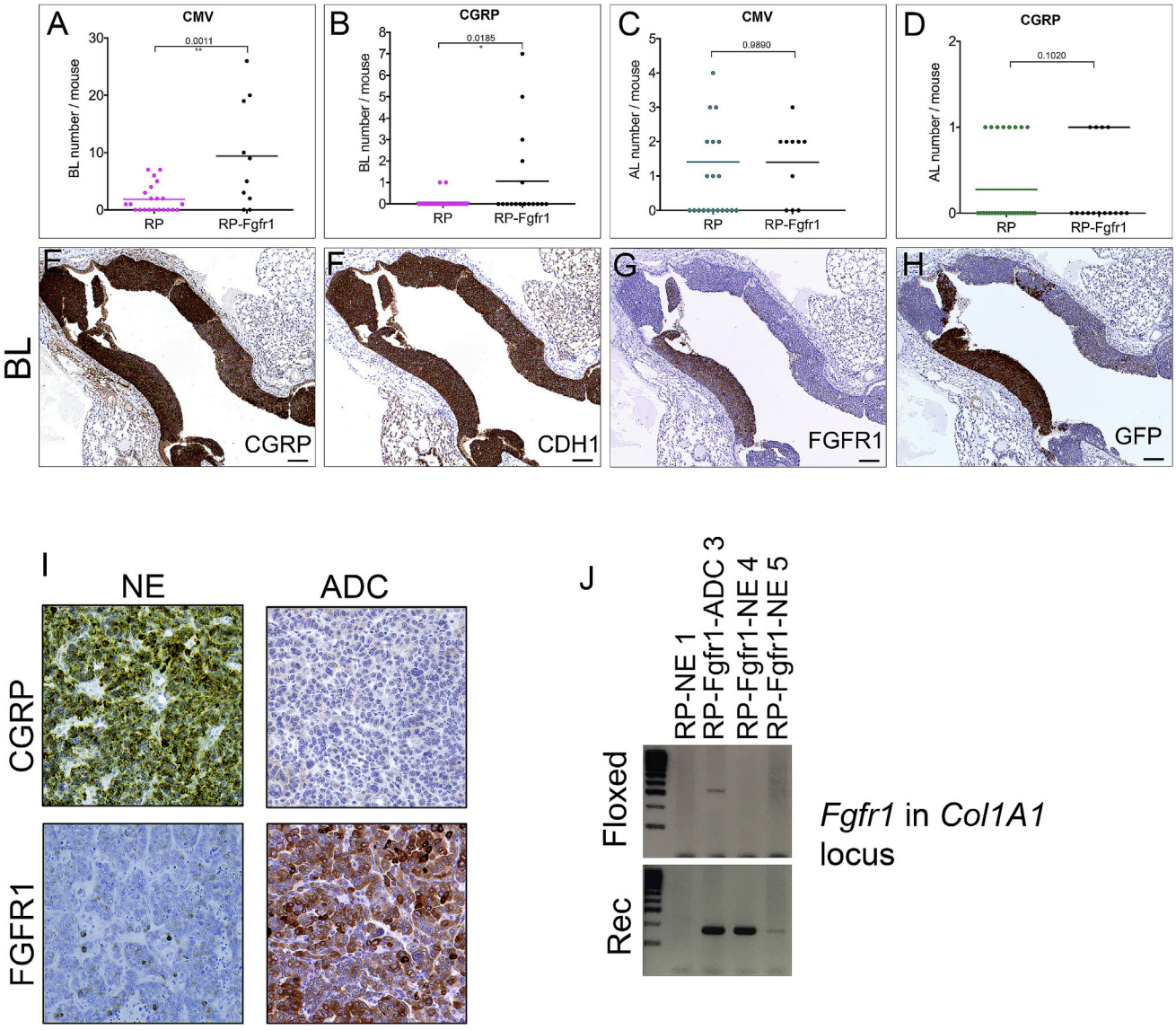

Figure 2. Bronchial Lesions Are Prominently Found in Ad5-CMV-Cre-Injected RP-Fgfr1 Mice

(A–D) Quantification of BLs (A and B) and ALs (C and D) in either Ad5-CMV-Cre (CMV; A and C) or Ad5-CGRP-Cre (CGRP; B and D)-injected *RP* and *RP-Fgfr1* mice.

(E–H) A representative BL of *RP-Fgfr1* mice stained for CGRP (E), CDH1 (F), FGFR1 (G), GFP (H). Scale bar, 100 μm.

(I) CGRP and FGFR1 staining of NE (left) and ADC lesions (right) of *RP-Fgfr1* mice injected with Ad5-CMV-Cre and collected at Humane Endpoint.

(J) PCR analysis on genomic DNA isolated from lung lesions (NE and ADC) of *RP* and *RP-Fgfr1* mice. Two Primer sets were designed to distinguish floxed from recombinant (Rec) *Fgfr1* alleles in the *Col1A1* locus. As expected, both primer sets did not give any PCR product when DNA from *RP* mice was used as negative control, whereas in both NE (RP-Fgfr1-NE 4, RP-Fgfr1-NE 5) and ADC (RP-Fgfr1-ADC 3) lesions of *RP-Fgfr1* mice, the primer set for the Rec *Fgfr1* allele gave a PCR product of the proper length. The primer set for the floxed allele gave only a faint band in the line of ADC sample. The image is representative of n = 2 ADC samples and n = 4 SCLC samples.

efficient. Therefore, the absence of FGFR1^{K656E} protein expression is likely the result of silencing of the allele by epigenetic mechanisms. Due to insufficient material, we could not successfully isolate genomic DNA directly from BLs. However, the finding that a wide collection of samples either negative or positive to FGFR1 staining all showed a near-complete activating recombination of *Fgfr1* allele suggests that the same has likely happened for BLs.

The discovery that BLs were mostly found in mice injected with Ad5-CMV-Cre and only very rarely in mice injected with Ad5-CGRP-Cre (Figures 1E–1H, 2A, and 2B), points to the existence of an unknown cell of origin that does not express CGRP, but, upon deletion of *Rb1* and *Trp53*, activates CGRP expression.

To gain insight into the cell of origin of BLs, and in order to define these lesions molecularly, we performed RNA sequencing (RNA-seq) of BLs and compared their expression

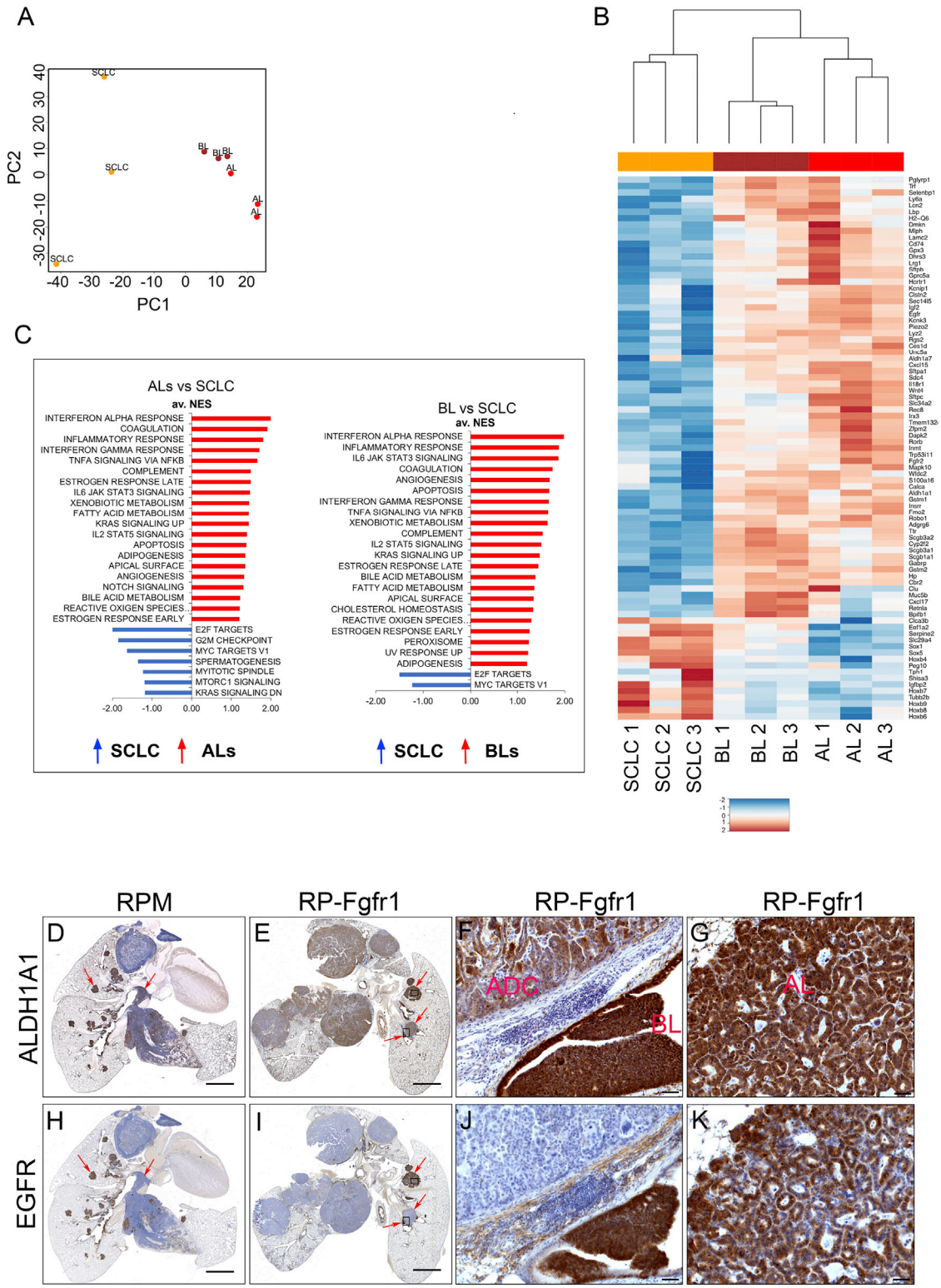

Figure 3. Bronchial Lesions Share the Molecular Circuitry with Cisplatin-Resistant Alveolar Lesions

(A) Principal component analysis on triplicates of SCLC, BLs, and ALs samples. Plotted are the principle components 1 and 2 (PC1, PC2).

(B) Heatmap of genes with the highest rotation value for PC1.

(legend continued on next page)

profile to SCLC and ALs. The expression profile of ALs has been described recently for cisplatin-treated Ad5-CMV-Cre-injected *RPM* (*Rb1*/*Trp53*/*Mycl*) mice (Böttger et al., 2019). For consistency, we isolated BLs from *RPM* mice and compared their expression profile with that of either ALs or SCLC of *RPM* mice. Our analysis identified 471 genes differentially expressed (DE) between SCLC and BLs, with 79 upregulated and 392 downregulated genes. We also compared SCLC to ALs and found a total of 834 DE genes, with 232 upregulated and 602 downregulated genes (Figures S2A, S2B, S2D, and S2E). The expression profile of BLs and ALs showed considerable overlap: only 81 genes were differentially expressed, with 52 downregulated and 29 upregulated genes in ALs lesions as compared to BLs (Figures S2C and S2F).

A principal component analysis (PCA) to determine the variance among all samples and also to define relationships between the three groups showed that BL and AL samples clustered in close proximity and distant from SCLC samples (Figure 3A). The list of genes included in the PC1 analysis revealed 70 commonly upregulated genes in ALs and BLs compared to SCLC and 15 genes commonly downregulated (Figure 3B). Among commonly upregulated genes, we found genes encoding transmembrane receptors involved in lung development, such as *Egfr*, *Fgfr2*, *Robo1*, and secreted factors, such as *Igf2* and *Wnt4* (Figure 3B).

Gene set enrichment analysis identified gene sets involved in xenobiotic metabolism and the oxidative stress response, such as aldehyde dehydrogenase family members (*Aldh1a1*, *Aldh1a7*), glutathione S-transferase family members (*Gstm1*, *Gstm2*), and cytochrome P450 2f2 (*Cyp2f2*) (Figures 3B and 3C).

Among other commonly upregulated gene sets in BLs and ALs versus SCLC, we found INNATE IMMUNE RESPONSE and KRAS SIGNALING UP, which suggest an involvement of MAPK pathway in both low-grade NE lesions compared to SCLC.

Gene set enrichment analysis of downregulated genes in ALs versus SCLC identified, among the most negatively enriched gene sets, E2F TARGETS, G2M CHECKPOINT, MYC TARGETS V1, mTORC1 SIGNALING, and MITOTIC SPINDLE (Figure 3C). In BLs versus SCLC, we found the same downregulated gene sets, but only E2F TARGETS and MYC TARGETS V1 were prominently downregulated (false discovery rate [FDR] <0.25).

Taken together, our sequencing data show that the expression profile of BLs greatly overlaps with that of ALs. In both cases, we found gene profiles suggesting reduced proliferation and altered metabolism. The remarkable difference of these low-grade NE lesions with SCLC suggests that they represent a distinct class of neoplastic lesions and, most importantly, that they have a different cell of origin.

In order to assess whether BLs and ALs of *RP-Fgfr1* mice share the expression profile of low-grade NE lesions found in *RPM* mice, we performed immunostaining for ALDH1A1 and EGFR, which were highly expressed in BLs and ALs compared to SCLC in *RPM* mice (Figures 3D and 3H). Although the overall lung phenotype of *RP-Fgfr1* mice appeared very different from that of *RPM* mice, mainly because of the reduced SCLC and the presence of LADC (Figures 3D and 3E), we detected enhanced expression of ALDH1A1 in BLs and ALs (Figures 3E–3G); BLs and ALs of *RP-Fgfr1* mice also showed high levels of EGFR, this in striking difference with LADC (Figures 3I–3K).

Our data indicate that low-grade NE lesions found in *RP-Fgfr1* mice likely represent the same type of lesions found in *RPM* mice and are histologically indistinguishable from lesions found in the BLs and ALs in the various genotypes. Only the frequency in which these lesions occur appears to be influenced by the additional driver genes and the cell-type specificity of the promoter driving Cre in the adenoviral vectors (Table S11).

The notion that our expression data did not reveal any gene signature specific for known lung cell subtypes suggests that the target cells do not constitute an identified lung progenitor cell. More detailed future investigations are required to address this issue.

FGFR1^{K656E} Expression Drives the Transformation of K14-Expressing Cells into SCLC and, to a Lesser Extent, ADC

Because our aim was to gain insight into the role of FGFR1 in human SCLC, it appeared critical to identify the lung cell compartment sensitive to transformation into SCLC upon FGFR1-mediated signaling. Hence, we targeted a larger array of distinct lung cell lineages using an additional set of adenoviral vectors permitting Cre recombinase-mediated switching, specifically in K14-, SPC-, and CC10-expressing cells.

Injection of *RP* and *RP-Fgfr1* mice with Ad5-K14-Cre specifically causes recombination in basal cells (Ferone et al., 2016). Remarkably, both *RP* and *RP-Fgfr1* mice developed SCLC with a penetrance of 60% and 50%, respectively (Tables S5 and S6). Tumors were invasive in both *RP* and *RP-Fgfr1* mice (Figures 4A, 4B, 4D, and 4E). Invariably, we found intrapulmonary dissemination (IPD) of SCLC (Tables S5 and S6). *RP-Fgfr1* mice also developed LADCs that were completely absent in *RP* mice (Figures 4A and 4D; Tables S5 and S6).

Tumor-free survival of *RP-Fgfr1* mice was shorter compared to *RP* mice (Figure 4G). We found peripheral low-grade NE lesions to be the major difference between Ad5-K14-Cre-injected *RP* and *RP-Fgfr1* mice. BLs and ALs were found in 33% and 58% of *RP-Fgfr1* mice, respectively, compared to 7% and 20% in *RP* mice (Tables S5 and S6). The number of BLs and ALs per mouse was also increased by FGFR1^{K656E} expression (Figures 4H and 4I). NE tumor burden was comparable between *RP* and *RP-Fgfr1* mice (Figure 4J). Contrary to CGRP^{POS} cells, K14^{POS}

(C) Gene set enrichment analysis (GSEA) using the HALLMARKS gene sets of ALs versus SCLC (left graph) and BLs versus SCLC (right graph); FDR q value <0.25, normalized enrichment score (NES) $\geq$1.

(D–K) ALDH1A1 (D–G) and EGFR (H–K) staining on lung sections indicating whole lung of *RP-Fgfr1* mice (E and I) and *RPM* mice as positive control (D and H) collected at humane endpoint. High magnification images of RP-Fgfr1 lungs show ALDH1A1 staining of ADC and BL (F) or AL (G) and EGFR staining of ADC and BL (J) or AL (K). Scale bars indicate 2 mm (D, E, H, and I) and 50 μm (F, G, J, and K). Arrows in (D) and (H) indicate central and peripheral lesions. Arrows in (E) and (I) indicate peripheral BL and AL lesions. Rectangles in (E) and (I) indicate regions that are shown with higher magnification in (F), (G), (J), and (K).
See also Figure S2.

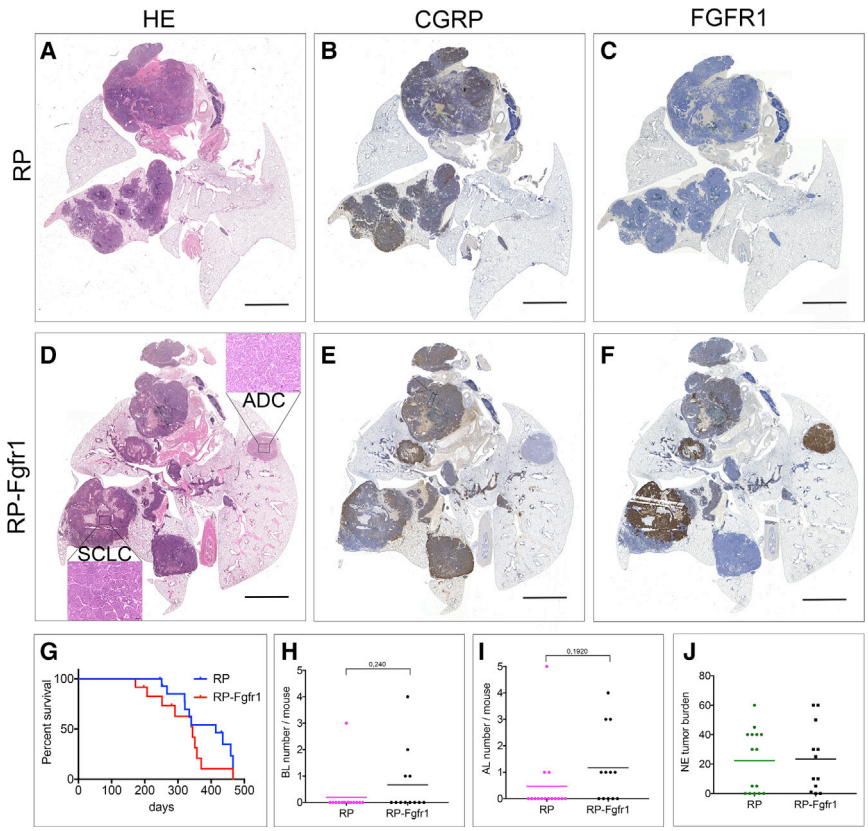

Figure 4. FGFR1 Overexpression Drives the Transformation of K14-Expressing Cells into SCLC and, to a Lesser Extent, ADC

(A–F) Scan image of HE (A and D), CGRP (B and E), and FGFR1 (C and F) staining of coronal sections of lungs from *RP* (A–C) and *RP-Fgfr1* mice (D–F) injected with Ad5-K14-Cre and collected at humane endpoint. Scale bar indicates 2 mm. Inset in (D) represents SCLC and the marginal ADC compartment. Scale bar inset indicates 50 μm.

(G) Lung cancer-free survival curve of mice with indicated genotypes.

(H–J) Quantification of BLs (H), ALs (I), and NE tumor burden (J) of mice with indicated genotypes.

See also Tables S5 and S6.

cells were tolerating high levels of FGFR1^{K656E} expression as assessed by immunostaining of *RP* and *RP-Fgfr1* lung (Figures 4C and 4F).

Taken together, our data show that in case of *RP-Fgfr1* mice, the primary cell of origin of SCLC is a K14^{POS} lung cell rather than the typical CGRP^{POS} NE cell, which has been considered the predominant SCLC initiating cell in all mouse models described to date. Our data also show that activation of FGFR1 signaling is able to promote BLs and ALs in K14-expressing cells although K14^{POS} cells might not be the exclusive cell of origin of these low-grade NE lesions.

FGFR1^{K656E} Expression Promotes Early Transformation of CC10^{POS} and SPC^{POS} Cells in LADC and Not SCLC

Because K14^{POS}, and not CGRP^{POS}, cells are the cell of origin of SCLC in *RP-Fgfr1* mice, we wanted to know whether other predominant lung cell lineages could also give rise to NE lesions and to what extent. Therefore, we specifically switched conditional alleles of *RP-Fgfr1* and *RP* control mice in club secretory cells by using Ad5-CC10-Cre and in alveolar type 2 (AT2) cells by using Ad5-SPC-Cre (Sutherland et al., 2011).

RP mice developed SCLC exclusively when either CC10^{POS} or SPC^{POS} cells were targeted (Figures 5A–5D). However, tumor onset was much slower as compared to *RP* mice injected with Ad5-CGRP-Cre, resulting, on average, in a longer survival (Tables S4, S8, and S10). *RP* mice injected with Ad5-CC10-Cre showed a tendency of an even lower penetrance of SCLC compared to *RP* mice injected with Ad-SPC-Cre (Tables S8 and S10) in line with previous observations (Table S12). Low-grade NE lesions were spuriously present in *RP* mice injected with Ad5-CC10-Cre and virtually absent in *RP* mice injected with Ad5-SPC-Cre (Tables S8 and S10).

The concomitant expression of FGFR1^{K656E} in either CC10^{POS} and SPC^{POS} cells gave rise to LADC (Figures 5E–5H). Due to the quick appearance of massive lesions of LADC in *RP-Fgfr1* mice (Figures 5K and 5L; Tables S7, S8, S9, and S10), we cannot exclude the potential for late onset of SCLC following Ad5-CC10-Cre and Ad5-SPC-Cre injection of *RP-Fgfr1* mice.

The penetrance of LADC was slightly lower upon Ad5-CC10-Cre injection (89%) as compared to 100% upon Ad5-SPC-Cre injection (Tables S7 and S9). Switched SPC^{POS} cells resulted in a higher tumor burden as compared to CC10^{POS} cells. This was the case both for SCLC in *RP* mice and for LADC in *RP-Fgfr1* mice (Figures 5I and 5J), although the difference was less pronounced for SCLC. The higher tumor burden of both *RP* and *RP-Fgfr1* mice injected with Ad5-SPC-Cre was associated with a shorter survival (Figures 5K and 5L).

Taken together, our data show that activation of FGFR1 in RB1 and TP53 deficient secretory club and AT2 cells is imposing LADC. AT2 cells seem more prone to transformation compared to club secretory cells, either into SCLC or LADC.

Gene Expression Profile of LADC Arising from SPC^{POS} and CGRP^{POS} Reveals Differences Associated with the Cell of Origin

We showed that Ad5-CGRP-Cre-injected *RP-Fgfr1* mice developed LADC (Figures 1K and 1L). In order to identify potential differences due to the distinct cells of origin giving rise to LADC, we compared the expression profile of LADC originating from SPC^{POS} cells and CGRP^{POS} cells with SCLC originating from CGRP^{POS} cells of *RP-Fgfr1* mice. Our aim was to identify commonly regulated genes associated with either

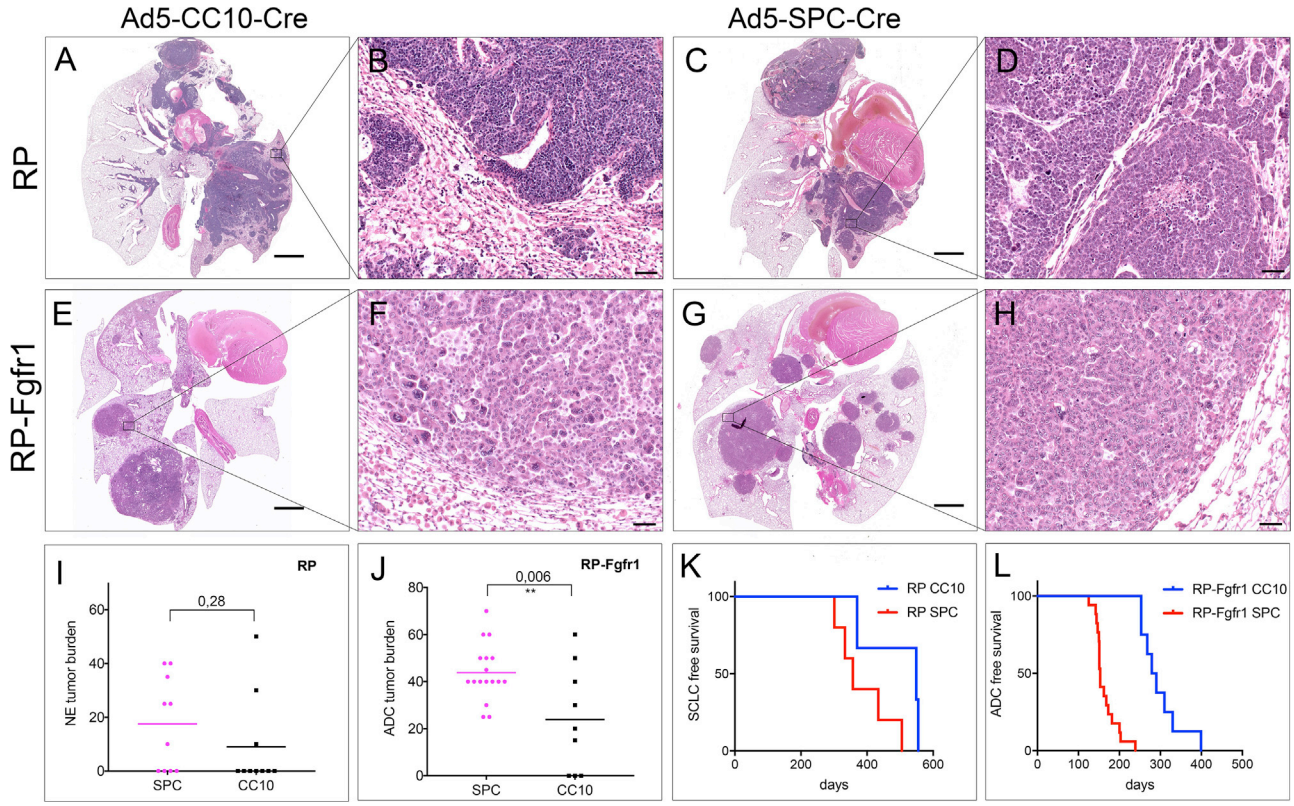

Figure 5. FGFR1^{K656E} Expression Promotes Early Transformation of CC10^{POS} and SPC^{POS} Cells in LADC and Not SCLC

(A–H) HE staining of RP (A–D) and *RP-Fgfr1* mice (E–H) injected with either Ad5-CC10-Cre (A, B, E, and F) or Ad5-SPC-Cre (C, D, G, and H) collected at humane endpoint. Images show the whole lung (A, E, C, and G) or ADC lesions at higher magnification (B, F, D, and H).

(I and J) NE tumor burden (I) and ADC tumor burden (J) of mice with the indicated genotypes.

(K) SCLC-free survival curve of RP mice injected with either Ad5-CC10-Cre (CC10) or AD5-SOC-Cre (SPC).

(L) ADC-free survival curve of RP-Fgfr1 mice injected with either Ad5-CC10-Cre (CC10) or AD5-SOC-Cre (SPC). Scale bars indicate 2 mm (A, C, E, and G) and 50 μm (B, D, F, and H).

See also Tables S7, S8, S9, and S10.

tumor histology (LADC from SPC^{POS} and CGRP^{POS} cells) or the cell of origin (LADC and SCLC originating from CGRP^{POS} cells).

Gene expression data showed that LADC samples, although originating from two different cells of origin, clustered together, while SCLC samples formed a distinct cluster (Figure S3A). We then performed a PCA on the data. The first principle component separated LADC and SCLC samples and explained 68% of the variation in the dataset (Figure 6A), not surprisingly the largest variation in the dataset.

We subsequently performed gene enrichment and functional analysis using the Database for Annotation, Visualization and Integrated Discovery (DAVID) program on the list of genes with major variation among samples extracted from PC1 (Figure S3B).

Among commonly upregulated genes in LADC versus SCLC, we mainly found genes involved in gas exchange such as *Sftpa1*, *Sftpb*, *Sftpc*, and *Sftpd*, and in the regulation of autophagy like *Dram1* and *Lamp3* (Figure S3B).

Downregulated genes were mostly represented by cellular functions associated to neuronal migration (*Lmx1b*, *Sox1*, *Celsr3*, and *Cdk5r2*), nerve-growth processing (*Pcsk1* and *Pcsk2*), secretion of neuropeptides (*Scg1* and *Scg2*), and secretory granule biogenesis (*Chga*). We also found downregulation of neuronal lineage genes like *Ascl1* and genes encoding for neuropeptides, such as *Calca*.

Taken together, our data show that LADC derived from either SPC^{POS} or CGRP^{POS} cells of *RP-Fgfr1* mice are very similar in terms of expression profile.

However, we also identified a number of DE genes common to LADC and SCLC originating from CGRP^{POS} cells versus LADC originating from SPC^{POS} cells (Figure 6B). Among the commonly upregulated genes in LADC and SCLC originating from CGRP^{POS} cells, we found genes involved in the oxidoreduction process (*Ndufs5*, *Ndufa12*, and *Ndufa1*), in DNA damage repair, metal ion binding, and most importantly, in neurogenesis, such as *Dlg3*, *Dab1*, and *Lhx2* (Figure 6B). Among the upregulated transcription factors, we found that *Sox2* was consistently upregulated in both LADC and SCLC originating from CGRP^{POS} cells as compared to LADC from SPC^{POS} cells (Figure 6B) and also confirmed by IHC staining (Figures 6F–6H); TTF1 staining is used as biomarker of LADC (Figures 6L–6N). Among the commonly downregulated genes in LADC and SCLC originating

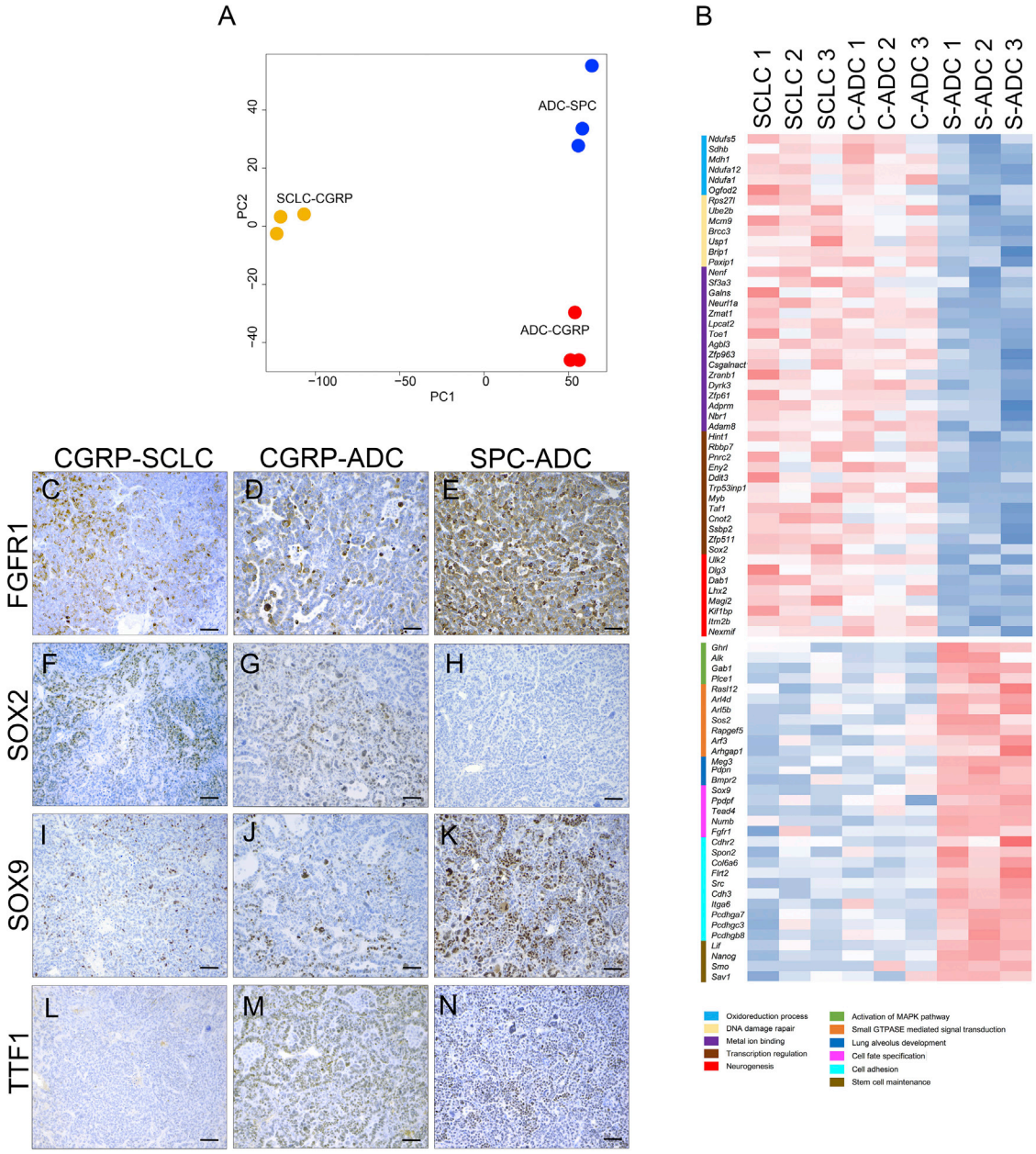

Figure 6. Gene Expression Profile of ADC Arising from SPC^{POS} and CGRP^{POS} Reveals Differences Associated with the Cell of Origin

(A) PCA analysis on triplicates of SCLC, ADC developed by Ad5-CGRP-Cre-injected *RP-Fgfr1* mice (SCLC-CGRP; ADC-CGRP), and ADC developed by Ad5-SPC-Cre-injected *RP-Fgfr1* mice (ADC-SPC), defined by variables PC1 and PC2.

(B) Heatmap of significantly (FDR <0.05) upregulated and downregulated genes between SCLC and ADC originating from CGRP^{POS} cells (C-ADC) versus ADC initiated from SPC^{POS} cells (S-ADC). Gene ontology and functional analysis performed with DAVID program identified the indicated terms (legend with different colors).

(C–N) FGFR1 (C–E), SOX2 (F–H), and SOX9 (I–K) staining on SCLC (CGRP-SCLC; C, F, I, and L) and ADC (CGRP-ADC; D, G, J, and M) developed by Ad5-CGRP-Cre-injected *RP-Fgfr1* mice, and ADC developed by Ad5-SPC-Cre-injected *RP-Fgfr1* mice (SPC-ADC; E, H, K, and N). TTF1 staining is used as positive control of ADC (L–N). Scale bar indicates 50 μm.

See also Figure S6.

from CGRP^{POS} cells, we found genes involved in the activation of MAPK pathway (*Alk*), lung alveolus development (*Pdpn*), cell adhesion (*Col6a6* and *Itga6*), stem cell maintenance (*Nanog* and *Lif*), and cell fate specification, such as *Sox9* and *Fgfr1*. The latter two were also confirmed by IHC (Figures 6C–6E and 6I–6K).

Our data indicate that FGFR1 signaling can drive initiation of LADC in CGRP^{POS} cells of *RP-Fgfr1* mice, whereas they also

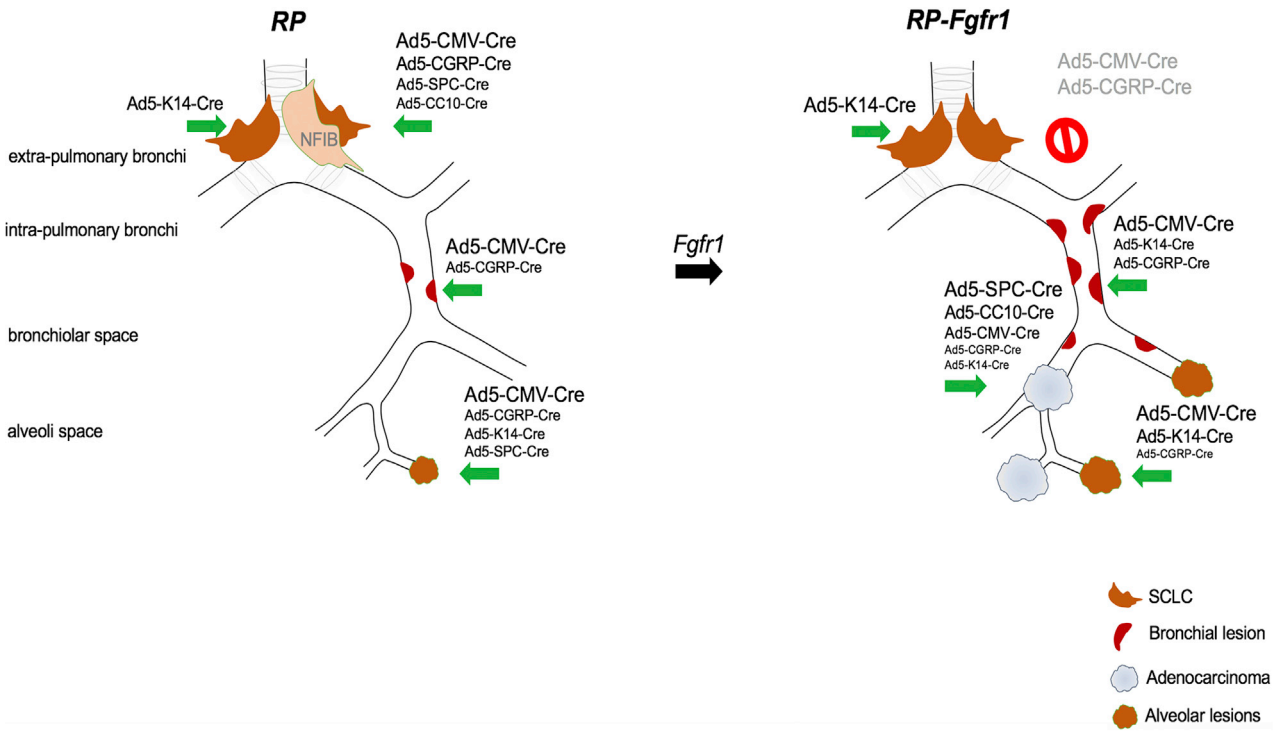

Figure 7. FGFR1 Is a Context-Dependent Oncogene

Schematic representation of neoplastic lesions developed according to the targeted cell type by *RP* mice and *RP-Fgfr1* mice: *RP* mice develop primarily typical central SCLC when $CGRP^{POS}$ cells are targeted; *RP* mice injected with Ad5-CMV-Cre also develop BLs and ALs, but their contribution to the tumor burden is very marginal. In *RP-Fgfr1* mice injected with any virus except Ad5-K14-Cre virus, the development of SCLC is inhibited. Peripheral NE lesions are promoted, especially when mice are injected with Ad5-CMV-Cre. *RP-Fgfr1* mice also develop ADC. Ad5-SPC-Cre- and Ad5-CC10-Cre-injected mice develop ADC exclusively, whereas ADC is quite marginal in Ad5-CGRP-Cre- and Ad5-K14-Cre-injected mice.

show that both SCLC and LADC originating from $CGRP^{POS}$ cells do not tolerate persistent FGFR1 signaling.

$FGFR1^{K656E}$ Promotes the Development of Tumors in the Nasal Cavity of RP-Fgfr1 Mice

Besides lung tumors, *RP-Fgfr1* mice injected with Ad5-CMV-cre, Ad5-CGRP-Cre, and Ad5-K14-Cre viruses also developed nasal tumors.

Strikingly, 64% of *RP-Fgfr1* mice (14 out of 22) injected with Ad5-CMV-Cre developed nasal tumors compared to only 15% (3 out of 19) of *RP* mice (Figure S4; Tables S1 and S2). Nasal tumors in both *RP* and *RP-Fgfr1* mice expressed synaptophysin (SYP), a recognized biomarker of NE tumors (Figures S4C and S4H). However, the nasal tumors from *RP-Fgfr1* mice showed a great degree of pleomorphism containing numerous single and multinucleated giant bizarre cells (Figures S4A, S4B, S4F, and S4G). In general, the nasal tumors of *RP-Fgfr1* mice were invasive and often grew into surrounding tissues and organs such as orbit, sinus, and even brain, whereas nasal tumors of *RP* mice were smaller and less invasive. As expected, nasal tumors of *RP-Fgfr1* mice expressed high levels of $FGFR1^{K656E}$ (Figures S4D and S4I); SOX2 expression was high only in the early nasal lesions of *RP* mice (Figures S4E and S4J).

Nasal tumors were found in 71% of *RP-Fgfr1* mice (19 out of 27) upon Ad5-CGRP-Cre injection (Tables S3 and S4) and not in *RP* mice (n = 20). However, nasal lesions originating from $CGRP^{POS}$ cells showed a later onset (Figure S4P), permitting development of lung tumors within the same time window. In line with Ad5-CMV-Cre-injected mice, nasal tumors originating from Ad5-CGRP-Cre-injected *RP-Fgfr1* mice appeared morphologically very similar (Figures S4K and S4L) showing NE differentiation as indicated by the consistent expression of SYN (Figure S4M), $FGFR1^{K656E}$ expression (Figure S4N), and marginal SOX2 expression (Figure S4O).

RP-Fgfr1 mice injected with Ad5-K14-Cre developed nasal tumors with a penetrance of 67%. The number of nasal samples collected from Ad5-K14-Cre-injected *RP* mice do not allow for a reliable estimation of the % of nasal tumors, which we believe is overestimated due to the low number of samples (2 out of 7) (Tables S5 and S6). Nasal tumors showed consistent NE differentiation: they expressed high levels of CGRP and SYN (data not shown).

Taken together, our data indicate that $FGFR1^{K656E}$ expression promotes the transformation of nasal epithelium cells into neoplastic lesions with NE differentiation.

$FGFR1^{K656E}$ Is a Context-Dependent Oncogene

RP mice injected with recombinant adenoviruses driving Cre expression, either ubiquitously (Ad5-CMV-Cre) or specifically in $CGRP^{POS}$, $K14^{POS}$, SPC^{POS}, and $CC10^{POS}$ lung cells,

consistently and exclusively developed NE lesions with the typical central SCLC as the most pronounced lesion, although the latency, penetrance, and number of lesions per mouse ranged from high (CMV) to low (CC10) (Figure 7; Tables S2, S4, S6, S8, S10, and S11). Data obtained by targeting $CGRP^{POS}$, SPC^{POS}, and $CC10^{POS}$ cells are in line with previous studies (Table S13). Expression of constitutively active FGFR1 dramatically affected the tumor phenotype of *RP* mice causing $CGRP^{POS}$ cells to be much more refractory in developing SCLC, whereas $K14^{POS}$ cells emerged as effective SCLC cells of origin of *RP-Fgfr1* mice (Figure 7; Tables S1, S3, S5, S7, S9, and S11).

RP-Fgfr1 mice developed peripheral low-grade bronchial and alveolar NE lesions most predominantly when Ad5-CMV-Cre was used to switch the conditional alleles and, to a lesser extent, when $CGRP^{POS}$ or $K14^{POS}$ cells were targeted (Figure 7). In contrast, *RP-Fgr1* mice developed LADC from any of the targeted cells: Ad5-SPC-Cre- or Ad5-CC10-Cre-injected mice developed LADC exclusively, whereas in Ad5-K14-Cre-injected mice, the LADC compartment was rather marginal, giving predominant rise to central and peripheral NE lesions (Figure 7).

Taken together, our data show that FGFR1 activation can promote different degrees of NE lesions and LADC depending on the cell of origin. Most importantly, they indicate that FGFR1 activation can inhibit SCLC when it originates from $CGRP^{POS}$ cells whereas it promotes SCLC when initiated from $K14^{POS}$ cells.

DISCUSSION

Here, we have studied how FGFR signaling, often observed as a result of amplification of the *FGFR1* gene in human SCLC, is associated with a distinct tumor phenotype and cell of origin. Therefore, we have generated a conditional dominant active allele of *Fgfr1* inserted in the *Col1A1* locus. Side-by-side comparison of mice carrying conditional *Rb1* and *Trp53* alleles (*RP*) with mice carrying on top the conditional mutant *Fgfr1* allele (*RP-Fgfr1*) have shown how FGFR1 signaling can influence tumor development in a *Rb1*;*Trp53*-deficient background. By using a set of previously described Ad5-Cre viruses, we have targeted these genetic lesions to specific subsets of lung cells and monitored tumor development.

Neuroendocrine Lung Tumors Can Originate from Different Cells in Lung

Previously, we and others have reported that SCLC in mice can be induced by Cre-mediated inactivation of *Rb1* and *Trp53* in a variety of lung cells (Table S13). Targeting lung cells by using the ubiquitous CMV promoter appeared the most efficient approach, followed by switching $CGRP^{POS}$ NE cells and SPC^{POS} cells, respectively (Sutherland et al., 2011). This, together with data of other investigators, who did not observe SCLC upon switching SPC^{POS} cells (Gazdar et al., 2017), has led to the view that lung NE cells represent the predominant cell of origin of SCLC.

Our results reveal that SCLC can originate from more cell lineages than previously assumed (Figure 7) e.g., inactivation of *Rb1* and *Trp53* in $K14^{POS}$ cells enables development of SCLC with a similar penetrance as found for $CGRP^{POS}$ cells.

Moreover, we observe a diversity of NE lesions when tumors are induced by a generally expressed CMV-Cre virus. This results in "typical" central lesions, most reminiscent of human SCLC and peripheral lesions that are more benign and found in the BL and AL space. BLs and ALs appear less aggressive with no evidence of local dissemination, although this might change as a result of additional lesions (Yang et al., 2018). These peripheral lesions are much more efficiently induced by the CMV-Cre virus than by any of the other cell-type-specific Cre viruses. These observations align with those made for *RP* mice overexpressing *Mycl* (*RPM*) (Böttger et al., 2019) and *RP* mice with the additional inactivation of *Rbl2* (Yang et al., 2018).

Finally, comparing the expression profiles of these peripheral lesions that are more abundant in *RPM* mice with typical central SCLC tumors showed distinct differences as illustrated by principal component analysis (Figure 3A). We conclude that NE lesions induced in the bronchiolar and alveolar space represent closely related entities that significantly differ from more centrally located SCLC. Concomitant *Fgfr1* signaling enhances the penetrance and the number per mouse of these NE peripheral lesions while retaining their more benign *in situ* character. Apparently, it requires additional driver lesions such as *p130* loss or *Nfib* overexpression to transform these peripheral tumors in more aggressive metastasizing tumors (Yang et al., 2018).

Overexpression of $FGFR^{K656E}$ Promotes Low-Grade NE Lesions

We observe more BLs and ALs when *RP* mice express $FGFR1^{K656E}$ although there appears selection against its continued expression. The observation that these peripheral lesions are most predominant when CMV-Cre virus is used while virtually absent when Cre is delivered in AT2 or Club cells indicates that cells not previously identified serve as the cells of origin of these tumors.

As indicated by the gene expression analysis, the unique features of these tumors are further substantiated by distinct expression markers that distinguish them from the typical central SCLC lesions. For instance, both BLs and ALs of *RPM* and *RP-Fgfr1* mice express high levels of ALDH1 and EGFR. A high level of ALDH1 has been previously related to stem cell properties in LADC (Huang et al., 2013; Ji et al., 2014; Jiang et al., 2009). In line with this observation, *RP-Fgfr1* mice showed expression of ALDH1, also in LADC (Figure 3F), whereas even higher levels of ALDH1 are seen in BLs and ALs (Figure 3F), suggesting that an "$ALDH1^{high}$ cancer stem cell population" likely gives rise to these low-grade NE lesions. We also observed high levels of EGFR in ALs and BLs: EGFR has been reported as amplified in human bronchial carcinoids (Voortman et al., 2010), suggesting that NE peripheral lesions we describe here resemble human carcinoids.

The observation that these peripheral lesions gradually lose $FGFR1^{K656E}$ expression suggests that FGFR1 plays a role during initiation of these tumors, but subsequently, its expression is poorly tolerated. This is reminiscent of the situation observed in human LADC carrying EGFR mutations in which treatment

with EGFR inhibitors can result in transdifferentiation to SCLC that shows impaired MAPK signaling (Niederst et al., 2015). We have previously observed that forced expression of mutant KRAS is poorly tolerated by SCLC cells, resulting in loss of NE marker profile and acquisition of NSCLC phenotype (Calbo et al., 2011). The apparent mutual exclusiveness of sustained MAPK signaling with NE features is particularly intriguing in view of the notion that a fraction of the SCLC show amplification of the *FGFR1* gene. As we will argue below, this appears dictated by the cell of origin and both applies to SCLC as well as LADC.

Overexpression of FGFR ^{K656E} Impairs SCLC Initiated from NE CGRP^{POS} while Promoting SCLC Initiated from K14^{POS} Epithelial Cells

Whereas FGFR1^{K656E} promoted the initiation of peripheral lesions, it strongly impaired typical central SCLC development when induced by either CMV-Cre or CGRP-Cre viruses. Because we used time-matched mice for these comparisons, this cannot be ascribed to differences in mice survival. As observed for SCLC cell lines, which show intolerance to constitutive MAPK signaling, CGRP^{POS} cells apparently do not tolerate FGFR1 signaling well. Central lesions arising following Ad5-CGRP-Cre instillation of *RP-Fgfr1* mice did not show expression of FGFR1^{K656E} (Figures 6B and 6C). Intriguingly, when tumors were induced by K14-Cre in either *RP* or *RP-Fgfr1* mice, SCLC was found in a substantial percentage of the mice. In this case, many of the tumors in *RP-Fgfr1* mice, but not in *RP* mice, expressed FGFR1^{K656E}, indicating that K14^{POS} cells of origin of SCLC might actually benefit from FGFR1^{K656E} expression. Therefore, central lesions can have distinct cells of origin with a differential tolerance to FGFR1 signaling. This might imply that human SCLC samples showing FGFR1 overexpression preferentially originate from a K14^{POS}, CGRP^{NEG} cell.

FGFR1 Catalyzes Development of LADC from a Wide Variety of Lung Cells

Given the differential effect of FGFR1^{K656E} expression on the induction of SCLC, we asked whether similar preferences also apply to the cell of origin of LADC. Therefore, we monitored LADC development in *RP* and *RP-Fgfr1* mice using the complete set of Cre viruses. In *RP* mice, LADC was virtually absent. Even Ad5-SPC-Cre virus failed to induce LADC. In contrast, LADC was found at high incidence in *RP-Fgfr1* mice irrespective of the virus used, although CMV, SPC, and CC10-Cre viruses were the most effective. Interestingly, CGRP-Cre and K14-Cre delivery also gave rise to LADC. LADC induced by CGRP-Cre virus did not express FGFR1^{K656E}, similarly to what we observed for SCLC, although its activation was clearly required for LADC development. Apparently, CGRP^{POS} cells do not tolerate continuous FGFR1^{K656E} expression, this in contrast to LADC induced by SPC, CC10, and K14-Cre viruses. A principal component analysis (PC1, Figure 6A) shows close resemblance of LADCs induced by either SPC-Cre or CGRP-Cre (PC1), whereas CGRP-Cre-induced LADC shared a number of markers specifically with CGRP-Cre-induced SCLC (PC2). This indicates that the cell of origin of LADC also imposes distinct expression requirements for tumor outgrowth.

RP and RP-Fgfr1 Mice Develop Tumors in the Nasal Cavity

All viruses except SPC-Cre and CC10-Cre induced NE tumors in the nasal cavity. This phenotype was much more pronounced in *RP-Fgfr1* mice than in *RP* mice using either CMV-Cre, CGRP-Cre, or K14-Cre viruses, indicating that FGFR1^{K656E} acts as a collaborating oncogenic lesion in the induction of NE lesions in the nasal cavity. Because this was a confounding factor in our analysis, we took care to always use age- and infection time-matched mice in comparing lung tumor incidence and phenotype to exclude the modifying influence of independent tumors arising in these mice as much as possible. This was also done for mice in which both SCLC and LADC were found concurrently.

Implications for Human SCLC and LADC

Our study illustrates that a larger variety of lung cell types can give rise to both NE tumors as well as LADC (Figure 7). Earlier, we have shown that lung squamous cell carcinoma can arise from most cell types in lung, resulting in tumors that are indistinguishable with respect to their expression pattern (Ferone et al., 2016). The most remarkable observation reported here is the differential effect of FGFR1 signaling on tumor development: depending on the cell of origin, it can either promote or impair SCLC development. Even when promoting the initiation of NE lesions, it appears to have an adverse effect in later phases of tumor development. This effect was observed for the peripheral NE BLs and ALs and was likely also responsible for the impairment of typical central SCLC originating from CGRP^{POS} cells. In contrast, SCLC induced by K14-Cre did not show any adverse effect of continued FGFR1 expression. Interestingly, LADC induced in *RP-Fgfr1* mice by CGRP-Cre virus did show very marginal FGFR1^{K656E} expression, although FGFR1^{K656E} was evidently required for its induction. This suggests that a subset of lung cells do not tolerate well sustained mutant FGFR1 expression at specific stages of tumor development. Because we used a constitutive active form of FGFR1, we cannot exclude that, upon FGFR1 amplification as seen in a subset of human SCLC, FGFR signaling is less pronounced and therefore not associated with some of the adverse effects of FGFR1^{K656E} expression we observed here. However, our observations indicate that the effects of inhibiting FGFR1 signaling in both SCLC and LADC are hard to predict, because the selective advantage conferred by aberrant FGFR signaling might be confined to the early stage of tumorigenesis. It will therefore be important to explore whether some of the markers that can distinguish these tumor subsets in the mouse have a counterpart in human SCLC and LADC and can be used in the future to assess whether they can serve as predictors for response to therapies.

STAR★METHODS

Detailed methods are provided in the online version of this paper and include the following:

- KEY RESOURCES TABLE
- LEAD CONTACT AND MATERIALS AVAILABILITY

SUPPLEMENTAL INFORMATION

Supplemental Information can be found online at https://doi.org/10.1016/j.celrep.2020.02.052.

ACKNOWLEDGMENTS

We thank the division of animal pathology Ellen Riem, Joost van Ooij, Lex de Vrije, and Jelrik van der Meer for producing high-quality histopathologic material and the animal facility for its support in maintaining the mice. This study was supported by European Research Council (319661 COMBATCANCER) and the Queen Wilhelmina Prize from the Dutch Cancer Society to A.B.

AUTHOR CONTRIBUTIONS

G.F. conceived the experiments and conducted most of them, coordinated the project, and wrote the paper. J.-Y.S. analyzed tumors and scored IHC staining. O.K. performed RNA-seq data analysis. J.v.d.V. and M.C. gave technical support for intratracheal injections. E.A.S. scored IHC staining. D.J.A. coordinated RNA sequencing. D.P. provided input in manuscript writing. A.B. supervised the whole project.

DECLARATION OF INTERESTS

The authors declare no competing interests.

Received: August 13, 2019
Revised: December 2, 2019
Accepted: February 11, 2020
Published: March 17, 2020

REFERENCES

Anders, S., Pyl, P.T., and Huber, W. (2015). HTSeq–a Python framework to work with high-throughput sequencing data. Bioinformatics *31*, 166–169.

Arrigoni, M.G., Woolner, L.B., and Bernatz, P.E. (1972). Atypical carcinoid tumors of the lung. J. Thorac. Cardiovasc. Surg. *64*, 413–421.

Böttger, F., Semenova, E.A., Song, J.Y., Ferone, G., van der Vliet, J., Cozijnsen, M., Bhaskaran, R., Bombardelli, L., Piersma, S.R., Pham, T.V., et al. (2019). Tumor heterogeneity underlies differential cisplatin sensitivity in mouse models of Small-Cell Lung Cancer. Cell Rep. *27*, 3345–3358.e4.

Calbo, J., van Montfort, E., Proost, N., van Drunen, E., Beverloo, H.B., Meuwissen, R., and Berns, A. (2011). A functional role for tumor cell heterogeneity in a mouse model of small cell lung cancer. Cancer Cell *19*, 244–256.

Cui, M., Augert, A., Rongione, M., Conkrite, K., Parazzoli, S., Nikitin, A.Y., Ingolia, N., and MacPherson, D. (2014). PTEN is a potent suppressor of small cell lung cancer. Mol. Cancer Res. *12*, 654–659.

Denny, S.K., Yang, D., Chuang, C.H., Brady, J.J., Lim, J.S., Grüner, B.M., Chiou, S.H., Schep, A.N., Baral, J., Hamard, C., et al. (2016). Nfib Promotes Metastasis through a Widespread Increase in Chromatin Accessibility. Cell *166*, 328–342.

Dobin, A., Davis, C.A., Schlesinger, F., Drenkow, J., Zaleski, C., Jha, S., Batut, P., Chaisson, M., and Gingeras, T.R. (2013). STAR: ultrafast universal RNA-seq aligner. Bioinformatics *29*, 15–21.

Ferone, G., Song, J.Y., Sutherland, K.D., Bhaskaran, R., Monkhorst, K., Lambooij, J.P., Proost, N., Gargiulo, G., and Berns, A. (2016). SOX2 Is the Determining Oncogenic Switch in Promoting Lung Squamous Cell Carcinoma from Different Cells of Origin. Cancer Cell *30*, 519–532.

Gazdar, A.F., and Brambilla, E. (2010). Preneoplasia of lung cancer. Cancer Biomark. *9*, 385–396.

Gazdar, A.F., Bunn, P.A., and Minna, J.D. (2017). Small-cell lung cancer: what we know, what we need to know and the path forward. Nat. Rev. Cancer *17*, 765.

George, J., Lim, J.S., Jang, S.J., Cun, Y., Ozretić, L., Kong, G., Leenders, F., Lu, X., Fernández-Cuesta, L., Bosco, G., et al. (2015). Comprehensive genomic profiles of small cell lung cancer. Nature *524*, 47–53.

Huang, C.P., Tsai, M.F., Chang, T.H., Tang, W.C., Chen, S.Y., Lai, H.H., Lin, T.Y., Yang, J.C., Yang, P.C., Shih, J.Y., and Lin, S.B. (2013). ALDH-positive lung cancer stem cells confer resistance to epidermal growth factor receptor tyrosine kinase inhibitors. Cancer Lett. *328*, 144–151.

Huijbers, I.J., Bin Ali, R., Pritchard, C., Cozijnsen, M., Kwon, M.C., Proost, N., Song, J.Y., de Vries, H., Badhai, J., Sutherland, K., et al. (2014). Rapid target gene validation in complex cancer mouse models using re-derived embryonic stem cells. EMBO Mol. Med. *6*, 212–225.

Iwakawa, R., Takenaka, M., Kohno, T., Shimada, Y., Totoki, Y., Shibata, T., Tsuta, K., Nishikawa, R., Noguchi, M., Sato-Otsubo, A., et al. (2013). Genome-wide identification of genes with amplification and/or fusion in small cell lung cancer. Genes Chromosomes Cancer *52*, 802–816.

Ji, Y., Zheng, M., Ye, S., Chen, J., and Chen, Y. (2014). PTEN and Ki67 expression is associated with clinicopathologic features of non-small cell lung cancer. J. Biomed. Res. *28*, 462–467.

Jiang, F., Qiu, Q., Khanna, A., Todd, N.W., Deepak, J., Xing, L., Wang, H., Liu, Z., Su, Y., Stass, S.A., and Katz, R.L. (2009). Aldehyde dehydrogenase 1 is a tumor stem cell-associated marker in lung cancer. Mol. Cancer Res. *7*, 330–338.

Kazanjian, A., Wallis, D., Au, N., Nigam, R., Venken, K.J., Cagle, P.T., Dickey, B.F., Bellen, H.J., Gilks, C.B., and Grimes, H.L. (2004). Growth factor independence-1 is expressed in primary human neuroendocrine lung carcinomas and mediates the differentiation of murine pulmonary neuroendocrine cells. Cancer Res. *64*, 6874–6882.

Koutsami, M.K., Doussis-Anagnostopoulou, I., Papavassiliou, A.G., and Gorgoulis, V.G. (2002). Genetic and molecular coordinates of neuroendocrine lung tumors, with emphasis on small-cell lung carcinomas. Mol. Med. *8*, 419–436.

Kwon, M.C., Proost, N., Song, J.Y., Sutherland, K.D., Zevenhoven, J., and Berns, A. (2015). Paracrine signaling between tumor subclones of mouse SCLC: a critical role of ETS transcription factor Pea3 in facilitating metastasis. Genes Dev. *29*, 1587–1592.

Love, M.I., Huber, W., and Anders, S. (2014). Moderated estimation of fold change and dispersion for RNA-seq data with DESeq2. Genome Biol. *15*, 550.

McFadden, D.G., Papagiannakopoulos, T., Taylor-Weiner, A., Stewart, C., Carter, S.L., Cibulskis, K., Bhutkar, A., McKenna, A., Dooley, A., Vernon, A., et al. (2014). Genetic and clonal dissection of murine small cell lung carcinoma progression by genome sequencing. Cell *156*, 1298–1311.

Meuwissen, R., Linn, S.C., Linnoila, R.I., Zevenhoven, J., Mooi, W.J., and Berns, A. (2003). Induction of small cell lung cancer by somatic inactivation of both Trp53 and Rb1 in a conditional mouse model. Cancer Cell *4*, 181–189.

Mills, S.E., Cooper, P.H., Walker, A.N., and Kron, I.L. (1982). Atypical carcinoid tumor of the lung. A clinicopathologic study of 17 cases. Am. J. Surg. Pathol. *6*, 643–654.

Niederst, M.J., Sequist, L.V., Poirier, J.T., Mermel, C.H., Lockerman, E.L., Garcia, A.R., Katayama, R., Costa, C., Ross, K.N., Moran, T., et al. (2015). RB loss in resistant EGFR mutant lung adenocarcinomas that transform to small-cell lung cancer. Nat. Commun. *6*, 6377.

Pardo, O.E., Arcaro, A., Salerno, G., Tetley, T.D., Valovka, T., Gout, I., and Seckl, M.J. (2001). Novel cross talk between MEK and S6K2 in FGF-2 induced proliferation of SCLC cells. Oncogene *20*, 7658–7667.

Pardo, O.E., Lesay, A., Arcaro, A., Lopes, R., Ng, B.L., Warne, P.H., McNeish, I.A., Tetley, T.D., Lemoine, N.R., Mehmet, H., et al. (2003). Fibroblast growth factor 2-mediated translational control of IAPs blocks mitochondrial release of Smac/DIABLO and apoptosis in small cell lung cancer cells. Mol. Cell. Biol. *23*, 7600–7610.

Pardo, O.E., Wellbrock, C., Khanzada, U.K., Aubert, M., Arozarena, I., Davidson, S., Bowen, F., Parker, P.J., Filonenko, V.V., Gout, I.T., et al. (2006). FGF-2 protects small cell lung cancer cells from apoptosis through a complex involving PKCepsilon, B-Raf and S6K2. EMBO J. *25*, 3078–3088.

Pardo, O.E., Latigo, J., Jeffery, R.E., Nye, E., Poulsom, R., Spencer-Dene, B., Lemoine, N.R., Stamp, G.W., Aboagye, E.O., and Seckl, M.J. (2009). The fibroblast growth factor receptor inhibitor PD173074 blocks small cell lung cancer growth in vitro and in vivo. Cancer Res. *69*, 8645–8651.

Park, K.S., Liang, M.C., Raiser, D.M., Zamponi, R., Roach, R.R., Curtis, S.J., Walton, Z., Schaffer, B.E., Roake, C.M., Zmoos, A.F., et al. (2011). Characterization of the cell of origin for small cell lung cancer. Cell Cycle *10*, 2806–2815.

Peifer, M., Fernández-Cuesta, L., Sos, M.L., George, J., Seidel, D., Kasper, L.H., Plenker, D., Leenders, F., Sun, R., Zander, T., et al. (2012). Integrative genome analyses identify key somatic driver mutations of small-cell lung cancer. Nat. Genet. *44*, 1104–1110.

Ravi, R.K., Weber, E., McMahon, M., Williams, J.R., Baylin, S., Mal, A., Harter, M.L., Dillehay, L.E., Claudio, P.P., Giordano, A., et al. (1998). Activated Raf-1 causes growth arrest in human small cell lung cancer cells. J. Clin. Invest. *101*, 153–159.

Ravi, R.K., Thiagalingam, A., Weber, E., McMahon, M., Nelkin, B.D., and Mabry, M. (1999). Raf-1 causes growth suppression and alteration of neuroendocrine markers in DMS53 human small-cell lung cancer cells. Am. J. Respir. Cell Mol. Biol. *20*, 543–549.

Rizvi, S.M., Goodwill, J., Lim, E., Yap, Y.K., Wells, A.U., Hansell, D.M., Davis, P., Selim, A.G., Goldstraw, P., and Nicholson, A.G. (2009). The frequency of neuroendocrine cell hyperplasia in patients with pulmonary neuroendocrine tumours and non-neuroendocrine cell carcinomas. Histopathology *55*, 332–337.

Rudin, C.M., Durinck, S., Stawiski, E.W., Poirier, J.T., Modrusan, Z., Shames, D.S., Bergbower, E.A., Guan, Y., Shin, J., Guillory, J., et al. (2012). Comprehensive genomic analysis identifies SOX2 as a frequently amplified gene in small-cell lung cancer. Nat. Genet. *44*, 1111–1116.

Schaffer, B.E., Park, K.S., Yiu, G., Conklin, J.F., Lin, C., Burkhart, D.L., Karnezis, A.N., Sweet-Cordero, E.A., and Sage, J. (2010). Loss of p130 accelerates tumor development in a mouse model for human small-cell lung carcinoma. Cancer Res. *70*, 3877–3883.

Semenova, E.A., Kwon, M.C., Monkhorst, K., Song, J.Y., Bhaskaran, R., Krijgsman, O., Kuilman, T., Peters, D., Buikhuisen, W.A., Smit, E.F., et al. (2016). Transcription Factor NFIB Is a Driver of Small Cell Lung Cancer Progression in Mice and Marks Metastatic Disease in Patients. Cell Rep. *16*, 631–643.

Sriuranpong, V., Borges, M.W., Ravi, R.K., Arnold, D.R., Nelkin, B.D., Baylin, S.B., and Ball, D.W. (2001). Notch signaling induces cell cycle arrest in small cell lung cancer cells. Cancer Res. *61*, 3200–3205.

Sutherland, K.D., and Berns, A. (2010). Cell of origin of lung cancer. Mol. Oncol. *4*, 397–403.

Sutherland, K.D., Proost, N., Brouns, I., Adriaensen, D., Song, J.Y., and Berns, A. (2011). Cell of origin of small cell lung cancer: inactivation of Trp53 and Rb1 in distinct cell types of adult mouse lung. Cancer Cell *19*, 754–764.

Tatematsu, A., Shimizu, J., Murakami, Y., Horio, Y., Nakamura, S., Hida, T., Mitsudomi, T., and Yatabe, Y. (2008). Epidermal growth factor receptor mutations in small cell lung cancer. Clin. Cancer Res. *14*, 6092–6096.

Travis, W.D. (2010). Advances in neuroendocrine lung tumors. Ann. Oncol. *21* (*Suppl 7*), vii65–vii71.

Voortman, J., Lee, J.H., Killian, J.K., Suuriniemi, M., Wang, Y., Lucchi, M., Smith, W.I., Jr., Meltzer, P., Wang, Y., and Giaccone, G. (2010). Array comparative genomic hybridization-based characterization of genetic alterations in pulmonary neuroendocrine tumors. Proc. Natl. Acad. Sci. USA *107*, 13040–13045.

Yang, D., Denny, S.K., Greenside, P.G., Chaikovsky, A.C., Brady, J.J., Ouadah, Y., Granja, J.M., Jahchan, N.S., Lim, J.S., Kwok, S., et al. (2018). Intertumoral Heterogeneity in SCLC Is Influenced by the Cell Type of Origin. Cancer Discov. *8*, 1316–1331.

STAR★METHODS

KEY RESOURCES TABLE

REAGENT or RESOURCE	SOURCE	IDENTIFIER
Antibodies		
Rabbit polyclonal anti-CGRP	Sigma-Aldrich	Cat# C8198; RRID: AB_259091
Rabbit monoclonal anti-CDH1	Cell Signaling Technology	Cat# 3195; RRID: AB_2291471
Rabbit monoclonal anti-FGFR1	Cell Signaling Technology	Cat# 9740; RRID: AB_11178519
Rabbit polyclonal anti-GFP	Abcam	Cat# ab6556; RRID: AB_305564
Rabbit polyclonal anti-ALDH1A1	Abcam	Cat# ab23375; RRID: AB_2224009
Rabbit monoclonal anti-EGFR	Abcam	Cat# ab52894; RRID: AB_869579
Rabbit polyclonal anti-SOX2	Millipore	Cat# AB5603; RRID: AB_2286686
Rabbit polyclonal anti-SOX9	Millipore	Cat# AB5535; RRID: AB_2239761
Mouse monoclonal anti-TTF1	Agilent	Cat# M357501-2; RRID: AB_2801260
Rabbit monoclonal anti-SYP	Abcam	Cat# ab32127; RRID: AB_2286949
Bacterial and virus strains		
Ad5-CMV-Cre	Viral Vector Core Facility, University of IOWA Health Care	N/A
Ad5-CGRP-Cre	Viral Vector Core Facility, University of IOWA Health Care	N/A
Ad5-K14-Cre	Viral Vector Core Facility, University of IOWA Health Care	N/A
Ad5-SPC-Cre	Viral Vector Core Facility, University of IOWA Health Care	N/A
Ad5-CC10-Cre	Viral Vector Core Facility, University of IOWA Health Care	N/A
Chemicals, Peptides, and Recombinant Proteins		
Cyclosporin A	Sigma-Aldrich	Cat# 30024
Deposited Data		
RNA-seq data	This paper	GEO: GSE132759
Experimental Models: Organisms/Strains		
Mouse: $Rb1^{flox/flox}$;$Trp53^{flox/flox}$	Meuwissen et al., 2003	N/A
Mouse: $Rb1^{flox/flox}$;$Trp53^{flox/flox}$; CAG < Lox66Mycl-LucLox71 >	Huijbers et al., 2014	N/A
Mouse: $Rb1^{flox/flox}$;$Trp53^{flox/flox}$; LSL-$Fgfr1^{K656E}$	This paper	N/A
Recombinant DNA		
Plasmid: LSL-$FGFR1^{K656E}$	Ferone et al., 2016	N/A
Software and Algorithms		
STAR (STAR_2.5.0c)	Dobin et al., 2013	https://github.com/alexdobin/STAR
HTSeq-count	Anders et al., 2015	https://htseq.readthedocs.io/en/release_0.11.1/
DESeq2	Love et al., 2014	http://bioconductor.org/packages/release/bioc/html/DESeq2.html
R (version 3.6.0)	https://www.r-project.org/contributors.html	https://www.r-project.org
AxioVision 4 software	Carl Zeiss Vision	N/A
GraphPad Prism, versions 7	GraphPad Software	https://www.graphpad.com
Other		
Zeiss Axioskop2 Plus microscope	Carl Zeiss Microscopy	N/A
Zeiss AxioCam HRc digital camera	Carl Zeiss Vision	N/A
HiSeq 2000 Sequencing System	Illumina	N/A

LEAD CONTACT AND MATERIALS AVAILABILITY

Further information and requests for resources and reagents should be directed to and will be fulfilled by the Lead Contact, Anton Berns (a.berns@nki.nl).

All unique/stable reagents generated in this study are available from the Lead Contact with a completed Materials Transfer Agreement.

EXPERIMENTAL MODEL AND SUBJECT DETAILS

Mice

All experiments involving animals were performed in accordance with Dutch and European regulations on care and protection of laboratory animals and have been approved by the local animal experiment committee at Netherlands Cancer Institute, DEC NKI (OZP ID 14016). All mice were maintained on an FVB background (backcrossed from strains generated from 129 Ola ESCs) and housed under standard condition of feeding, light and temperature with free access to food and water. Mice aged eight to ten weeks were used for experiments. Male and female mice were represented equally in the experimental cohorts and were group-housed (maximum 4 mice per cage) in individually ventilated cages (IVC) with standard enrichment.

We introduced *LSL-Fgfr1*^{K656E} allele directly into ES cells derived from *Rb1*$^{flox/flox}$;*Trp53*$^{flox/flox}$ mice, previously generated in our lab (Meuwissen et al., 2003), by performing Flp-recombinase mediated cassette exchange in the *Col1A1* locus.

METHOD DETAILS

Intratracheal Adenovirus instillation

Eight to ten weeks old mice were first treated with Cyclosporine A in drinking water (100 μg/ml) for immunosuppression, 1 week prior and 2 weeks following adenoviral injection. The day of virus injection mice were anesthetized with ketamine/sedazine and intratracheally injected with 20 μL of 1 × 10^{10} pfu/mL of purified adenovirus (Ad5-CMV-Cre, Ad5-CGRP-Cre, Ad5-K14-Cre, Ad5-SPC-Cre and Ad5-CC10-Cre; Viral Vector Core Facility, University of IOWA Health Care). Mice were monitored daily for signs of illness and culled upon respiratory distress or excessive weight loss (> 20% of initial weight).

Histology and Immunohistochemistry

For histological analysis, lungs were inflated and fixed for 24 h with ethanol–acetic acid–formalin (EAF). Fixed tissues were subsequently dehydrated, embedded in paraffin and sections of 2-4 μm were prepared, and stained with hematoxylin and eosin (H&E) for subsequent histopathological analyses. For IHC, tissue sections were rehydrated, blocked in BSA containing PBS, and sequentially incubated with specific primary antibodies and with biotinylated secondary antibodies (DAKO).

The following primary antibodies were applied: CGRP (Sigma, C8198),

E-cadherin/CDH1 (Cell signaling, 3195), FGFR1 (Cell signaling, 9740), GFP (Abcam, ab6556), ALDH1A1 (Abcam, ab23375), EGFR (Abcam, ab52894), SOX2 (Millipore, AB5603), SOX9 (Millipore AB5535), TTF1 (Agilent M357501-2), Synaptophysin/SYP (Abcam, ab32127).

The sections were reviewed with a Zeiss Axioskop2 Plus microscope (Carl Zeiss Microscopy, Jena, Germany) and images were captured with a Zeiss AxioCam HRc digital camera and processed with AxioVision 4 software (both from Carl Zeiss Vision, München, Germany).

RNA sequencing

RNA was isolated from laser capture micro-dissected paraffin sections of distinct lung lesions. 75bp paired-end RNA sequencing was performed on an Illumina HiSeq2000. Sequence reads were mapped to the mouse reference genome (*Mus musculus*, GRCm38) using STAR (STAR_2.5.0c) (Dobin et al., 2013). Mapped sequence reads were counted using HTSeq-count (Anders et al., 2015). Genes with False Discovery Rate (FDR) for differential expression lower than 0.05 were considered significant. Principal component analysis was performed using all genes in the dataset. To generate heatmaps related to the principle components the genes with an absolute rotation values four times higher than the standard deviation were selected.

QUANTIFICATION AND STATISTICAL ANALYSIS

Normalization and statistical analyses

Statistical analysis of the differential expression of genes was performed using DESeq2 (Love et al., 2014). All downstream analyses were performed in R (version 3.6.0) using the Bioconductor framework. The statistical methods used as well as the p values defining significance are stated in all figure legends referencing this data.

Survival analysis

Kaplan-Meier survival curves were analyzed using the log-rank test. All p values were calculated using a nonparametric Mann-Whitney test (statistical analyses were performed by GraphPad Prism, version 7).

Data visualization

Heatmaps were generated using the R-function heatmap.3 (https://github.com/obigriffith/biostar-tutorials/blob/master/Heatmaps/heatmap.3.R) using the z-score generated from RNA sequence read count data. Clustering was based on euclidean distance and complete linkage. PCA plots, GSEA-plots and volcano plots were generated in R (version 3.6.0). MAplots were generated using the 'plotMA' function from the DESeq2 R-package.

Expression plots were made using GraphPad Prism (version 7).

DATA AND CODE AVAILABILITY

The accession number for the sequencing data reported in this paper is Gene Expression Omnibus (GEO): GSE132759.

Cell Reports, Volume *30*

Supplemental Information

FGFR1 Oncogenic Activation Reveals an Alternative Cell of Origin of SCLC in Rb1/p53 Mice

Giustina Ferone, Ji-Ying Song, Oscar Krijgsman, Jan van der Vliet, Miranda Cozijnsen, Ekaterina A. Semenova, David J. Adams, Daniel Peeper, and Anton Berns

Supplemental Information

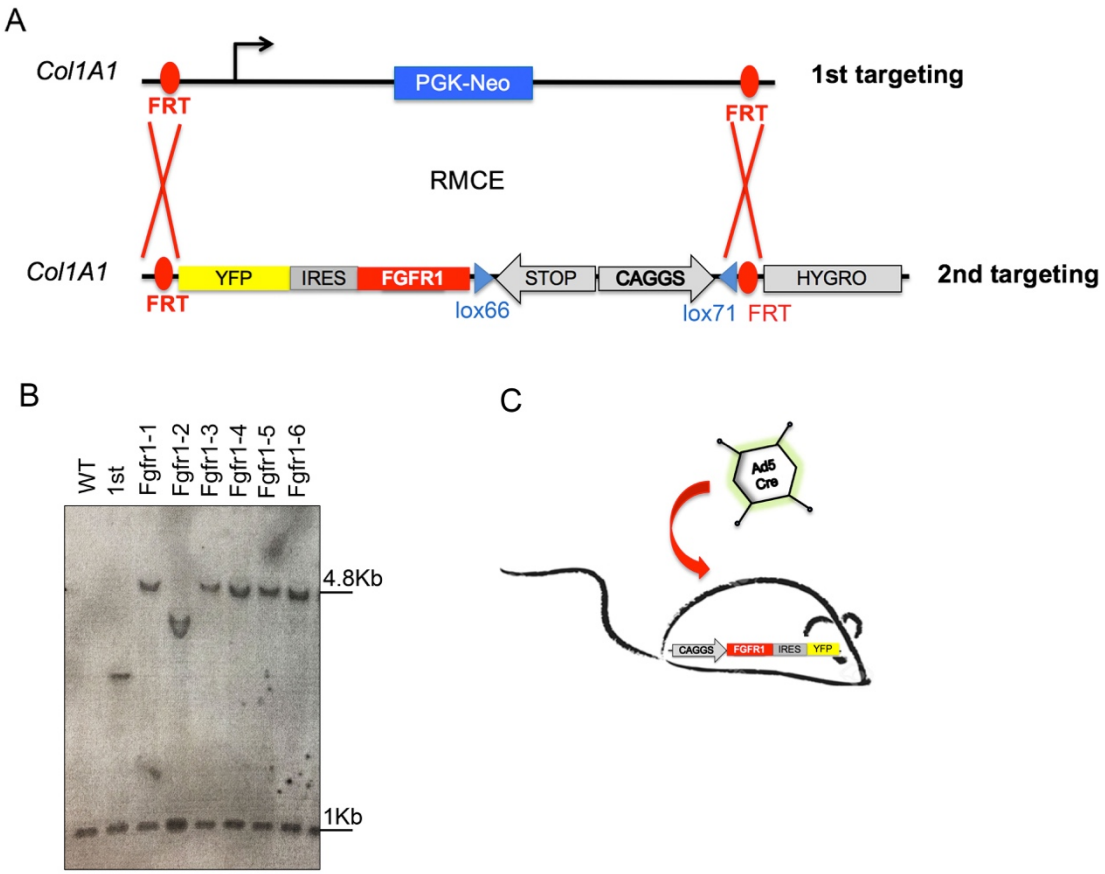

Figure S1. Related to Figure 1

(A) Schematic representation of the Flp-recombinase mediated cassette exchange (RMCE) technology: in the first step a cassette containing PGK-Neomycin flanked by FRT sites was targeted by homologous recombination to the *Col1A1* locus; in the second step, positive ES cell clones were transfected with a plasmid containing LSL-FGFR1^{K656E} followed by YFP and Flp recombinase, which mediated the cassette exchange.

(B) Southern blotting of BglII digested ES cells genomic DNA, hybridized to the *Col1A1* 3' probe, which anneals to a fragment of 1kb in wild-type mice (I line) and to a fragment of 4.9 kb in mice with a floxed allele. 5/6 Fgfr1 ES clones (Line 3 to 8) were heterozygote for the floxed allele. In line 2, an ES cell clone from the first targeting, was loaded as negative control.

(C) Mice are intratracheally injected with Adenoviruses carrying Cre recombinase in order to activate FGFR1^{K656E} expression in distinctive cell types.

Figure S2. Related to Figure 3

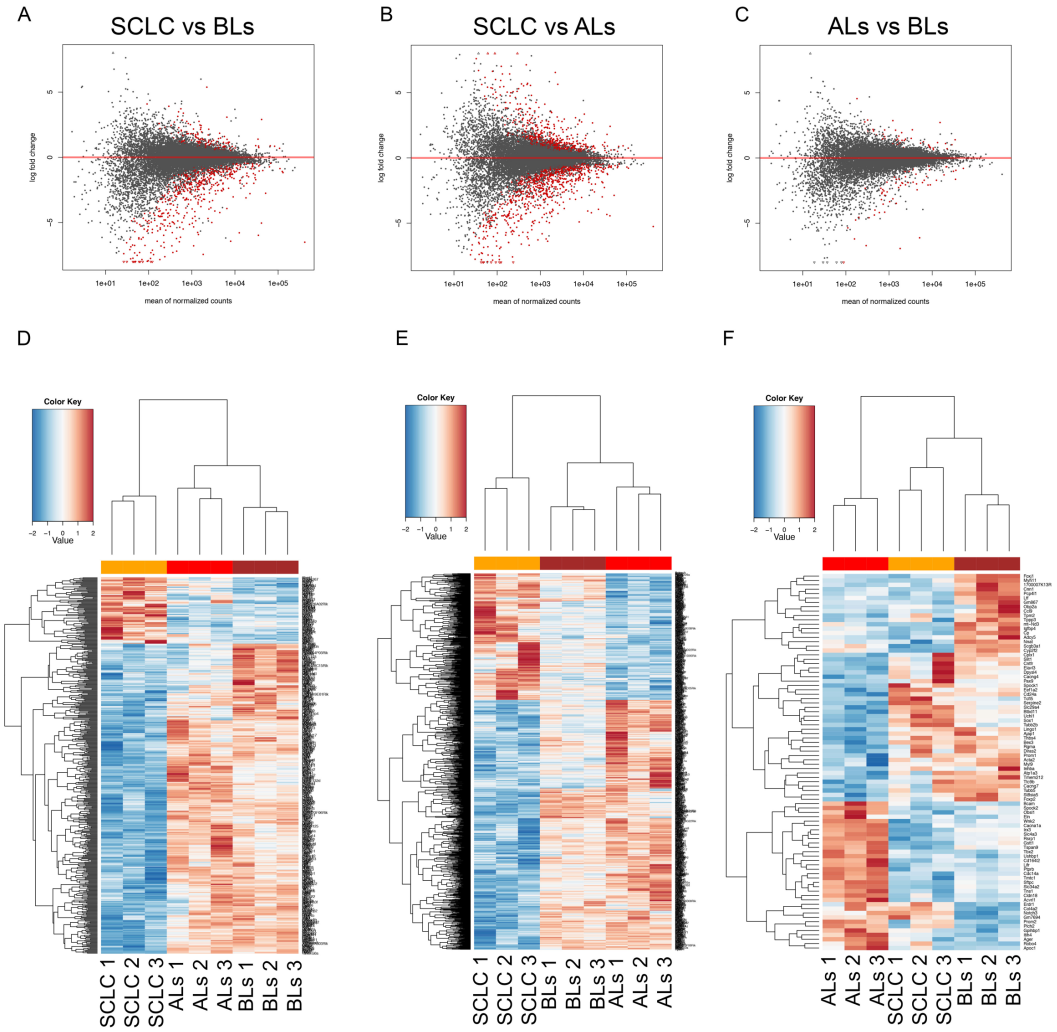

(A-C) MA-plot showing the log 2-fold change vs abundance of normalized gene expression of SCLC vs BLs (A), SCLC vs ALs (B), ALs vs BLs (C). Each point designates a gene; differentially expressed genes are in red. (D-F) Heatmap of significantly (FDR < 0.05) upregulated and downregulated genes in SCLC vs BLs (D), SCLC vs ALs (E), ALs vs BLs (F).

Figure S3. Related to Figure 6

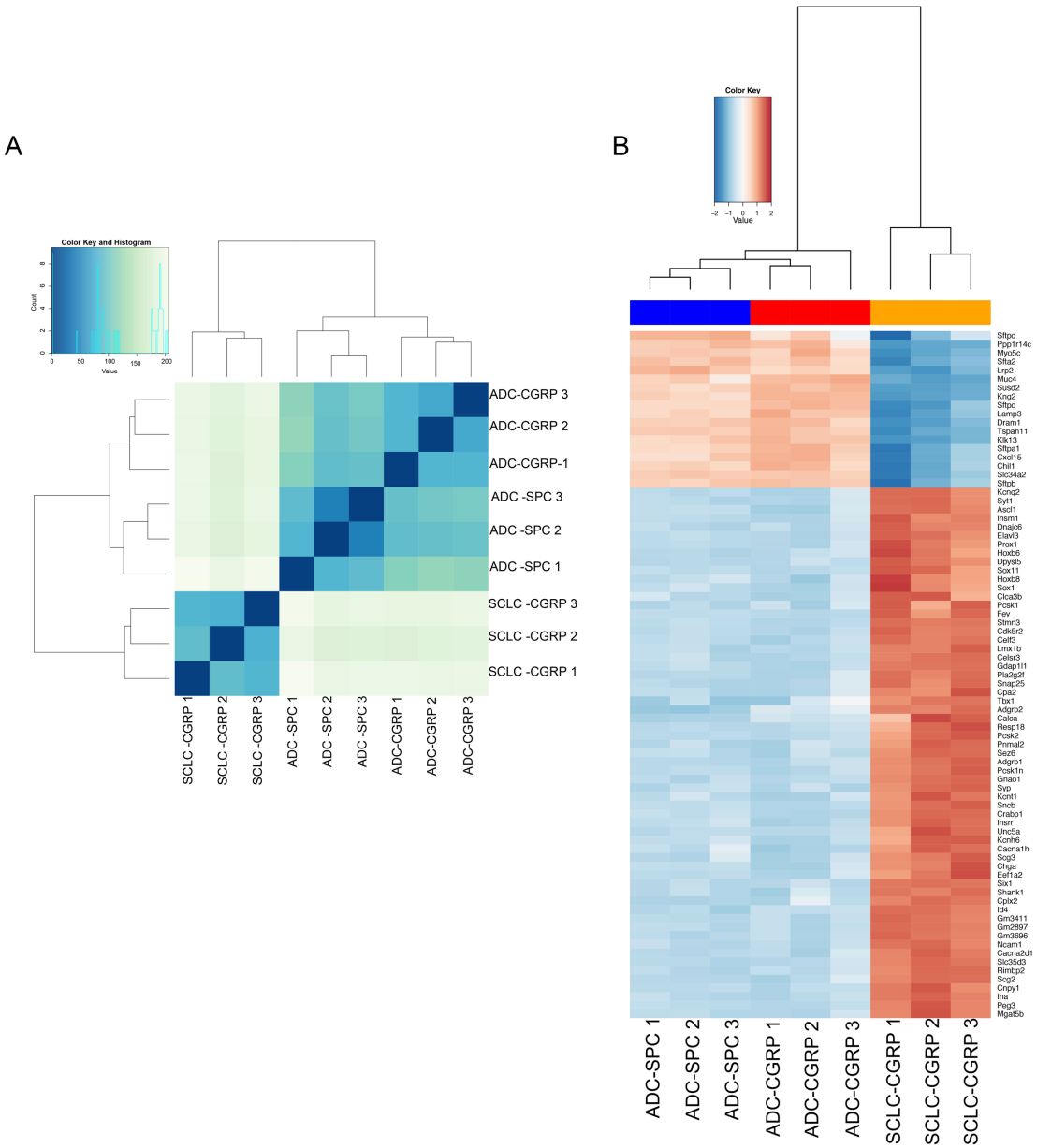

(A) Distance matrix and clustering of samples. Darkest color indicates lowest distance between samples. (B) Heatmap of genes with the highest rotation value for PC1.

Figure S4. Related to Figure 1

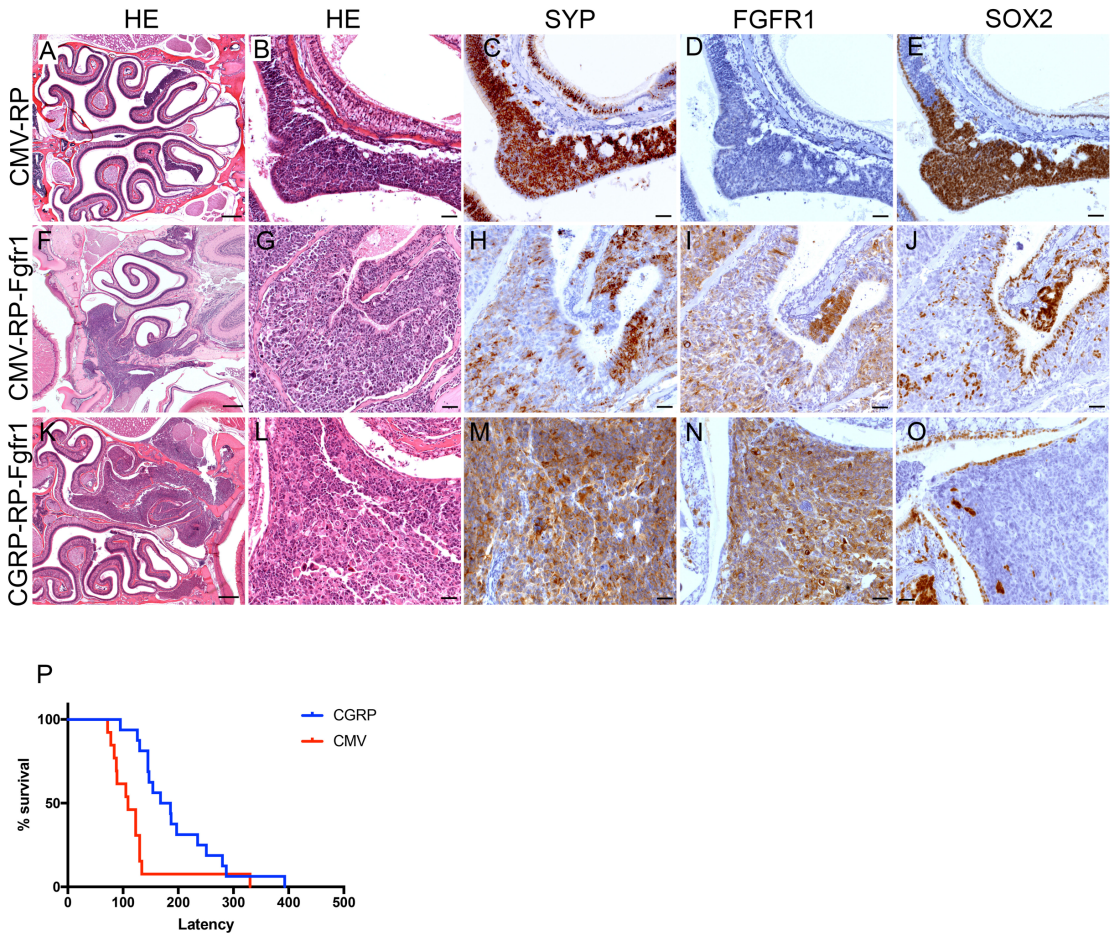

(A-T) HE, SYN, FGFR1, SOX2 staining on nasal sections of RP mice (A-E and K-O) and RP-fgfr1 mice (F-J and P-T) injected with either Ad5-CMV-Cre (CMV-RP and CMV-RP-Fgfr1, respectively) or Ad5-CGRP-Cre (CGRP-RP and CGRP-RP-Fgfr1, respectively). Scale bar, 50μm.

(U) Nasal tumor-free survival curve of RP-Fgfr1 mice injected with either Ad5-CGRP-Cre (CGRP) or Ad5-CMV-Cre (CMV).

Table S1. Neoplastic lesions developed by individual RP-Fgfr1 mice injected with Ad5-CMV-Cre. Related to Figure 1.

CMV	PROMAS	DAYS	SCLC	*IPD	*BL	*AL	*ADC	*NL
RP-Fgfr1	16GFE125	**72	-	-	+	-	+	+
RP-Fgfr1	16GFE050	78	-	-	+	-	-	+
RP-Fgfr1	16GFE051	84	-	-	-	-	-	+
RP-Fgfr1	16GFE067	88	-	-	+	+	-	+
RP-Fgfr1	16GFE068	89	-	-	-	+	-	+
RP-Fgfr1	16GFE077	105	-	-	+	-	-	+
RP-Fgfr1	16GFE148	109	-	-	-	-	-	+
RP-Fgfr1	15GFE229	123	-	-	-	-	-	+
RP-Fgfr1	16GFE160	123	-	-	+	+	+	+
RP-Fgfr1	16GFE096	130	-	-	+	+	+	+
RP-Fgfr1	16GFE163	130	-	-	+	+	+	+
RP-Fgfr1	16GFE074	134	-	-	-	-	-	+
RP-Fgfr1	16GFE080	144	-	-	+	+	+	-
RP-Fgfr1	15GFE255	150	-	-	+	+	+	-
RP-Fgfr1	16GFE098	162	-	-	+	-	+	-
RP-Fgfr1	15GFE286	173	-	-	-	+	+	-
RP-Fgfr1	16GFE135	179	-	-	+	+	+	-
RP-Fgfr1	15GFE285	187	-	-	+	+	+	-
RP-Fgfr1	15GFE291	189	+	-	+	-	+	-
RP-Fgfr1	16GFE150	231	-	-	+	+	+	+
RP-Fgfr1	16GFE042	330	+	-	+	+	-	+
RP-Fgfr1	16GFE062	393	-	-	-	-	-	-
		105,41	0%	0%	58,33%	41,67%	33,33%	***63,63%
		213,8	20%	0%	80%	70%	80%	

*IPD: intrapulmonary dissemination; BL: bronchial lesions; AL: alveolar lesions; ADC: Adenocarcinoma.; NL: nasal lesions.

**Samples depicted in beige indicate mice that died prematurely due to other phenotypes (e.g. nasal tumor) and therefore did not live long enough to develop lung tumors with an expected longer latency such as SCLC. For this reason, we calculated two different penetrance, depicted as well in beige or in white, according to the considered mouse group.

***Nasal tumor are independent from lung tumors and have a much shorter latency, therefore their penetrance is calculated on the total mouse number.

Table S2. Neoplastic lesions developed by individual RP mice injected with Ad5-CMV-Cre. Related to Figure 1

CMV	PROMAS	DAYS	SCLC	*IPD	*BL	*AL	*ADC	*NL
RP	16GFE092	**123	-	-	+	-	-	+
RP	16GFE109	169	-	-	+	+	-	NA
RP	16GFE110	169	-	-	+	-	-	NA
RP	17GFE042	191	+	+	-	+	-	+
RP	16GFE128	199	+	+	+	+	-	-
RP	16GFE152	208	+	+	+	-	-	-
RP	16GFE154	208	+	+	-	-	-	-
RP	17GFE079	219	+	+	+	+	-	-
RP	16GFE127	223	+	+	-	-	-	-
RP	16GFE023	231	+	+	-	+	-	-
RP	16GFE026	235	+	+	-	-	-	NA
RP	16GFE141	244	+	+	+	+	-	-
RP	16GFE142	244	+	+	+	+	-	-
RP	16GFE144	245	+	+	+	-	-	-
RP	17GFE103	247	+	+	+	-	-	-
RP	16GFE162	249	+	+	-	+	-	-
RP	16GFE032	260	+	+	-	+	-	-
RP	16GFE034	260	+	+	-	+	-	-
RP	17GFE001	266	+	+	+	-	-	+
RP	16GFE035	267	+	+	-	+	-	-
RP	16GFE166	277	+	+	-	-	-	-
RP	17GFE009	298	+	+	+	-	-	-
RP	17GFE041	333	+	+	+	-	-	-
			NA	NA	NA	NA	NA	***15%
		238,27	90%	90%	54,54%	50%	0%	

*IPD: intrapulmonary dissemination; BL: bronchial lesions; AL: alveolar lesions; ADC: Adenocarcinoma.; NL: nasal lesions.

**Samples depicted in beige indicate mice that died prematurely due to other phenotypes (e.g. nasal tumor) and therefore did not live long enough to develop lung tumors with an expected longer latency such as SCLC. For this reason, we calculated two different penetrance, depicted as well in beige or in white, according to the considered mouse group.

***Nasal tumor are independent from lung tumors and have a much shorter latency, therefore their penetrance is calculated on the total mouse number.

Table S3. Neoplastic lesions developed by individual RP-Fgfr1 mice injected with Ad5-CGRP-Cre. Related to Figure 1.

CGRP	PROMAS	DAYS	SCLC	*IPD	*BL	*AL	*ADC	*NL
RP-Fgfr1	16GFE069	**95	-	-	-	-	-	+
RP-Fgfr1	16GFE149	112	-	-	-	-	-	-
RP-Fgfr1	16GFE070	126	-	-	-	-	-	+
RP-Fgfr1	16GFE095	130	-	-	-	-	-	+
RP-Fgfr1	16GFE168	142	-	-	-	-	-	-
RP-Fgfr1	16GFE170	142	-	-	-	-	-	+
RP-Fgfr1	16GFE169	142	-	-	-	-	-	+
RP-Fgfr1	16GFE171	142	-	-	+	-	-	-
RP-Fgfr1	15GFE252	145	-	-	-	-	-	+
RP-Fgfr1	15GFE253	145	-	-	-	-	-	+
RP-Fgfr1	16GFE081	147	-	-	-	-	-	+
RP-Fgfr1	16GFE112	154	-	-	-	-	-	+
RP-Fgfr1	16GFE103	168	-	-	-	-	-	+
RP-Fgfr1	17GFE046	186	-	-	-	-	-	+
RP-Fgfr1	15GFE284	187	-	-	-	-	-	+
RP-Fgfr1	16GFE145	193	-	-	-	-	-	+
RP-Fgfr1	16GFE147	197	-	-	+	+	+	+
RP-Fgfr1	16GFE007	207	-	-	+	-	-	+
RP-Fgfr1	17GFE094	235	-	-	+	-	+	+
RP-Fgfr1	17GFE099	238	-	-	-	+	-	-
RP-Fgfr1	17GFE006	251	-	-	-	+	-	+
RP-Fgfr1	17GFE013	280	-	-	-	-	-	+
RP-Fgfr1	16GFE033	287	-	-	-	-	+	-
RP-Fgfr1	16GFE040	280	-	-	-	-	-	+
RP-Fgfr1	17GFE155	304	-	-	-	-	+	-
RP-Fgfr1	16GFE047	356	+	+	+	+	+	-
RP-Fgfr1	17GFE198	375	+	+	-	+	+	-
RP-Fgfr1	16GFE057	393	+	+	+	+	-	+
RP-Fgfr1	16ESE019	416	-	-	-	-	+	NA
		135,17	0%	0%	8%	0%	0%	***71,42%
		267,82	17,64%	17,64%	29,41%	35,29%	41,17%	

*IPD: intrapulmonary dissemination; BL: bronchial lesions; AL: alveolar lesions; ADC: Adenocarcinoma.; NL: nasal lesions.

**Samples depicted in beige indicate mice that died prematurely due to other phenotypes (e.g. nasal tumor) and therefore did not live long enough to develop lung tumors with an expected longer latency such as SCLC. For this reason, we calculated two different penetrance, depicted as well in beige or in white, according to the considered mouse group.

***Nasal tumor are independent from lung tumors and have a much shorter latency, therefore their penetrance is calculated on the total mouse number.

Table S4. Neoplastic lesions developed by individual RP mice injected with Ad5-CGRP-Cre. Related to Figure 1.

CGRP	PROMAS	DAYS	SCLC	*IPD	*BL	*AL	*ADC	*NL
RP	16GFE102	168	-	-	-	-	-	NA
RP	16GFE104	168	-	-	-	-	-	NA
RP	16GFE105	168	-	-	-	-	-	NA
RP	16GFE116	201	-	-	-	-	-	NA
RP	17GFE098	235	+	-	-	+	-	-
RP	16GFE143	245	-	-	-	-	-	-
RP	16GFE164	249	-	-	-	-	+	-
RP	17GFE113	249	-	-	-	-	-	-
RP	17GFE118	259	-	-	-	-	-	-
RP	17GFE131	268	+	-	+	+	-	-
RP	17GFE036	271	+	+	-	-	-	NA
RP	17GFE135	273	+	-	-	-	-	-
RP	17GFE142	284	+	+	-	-	-	-
RP	15ESE030	288	+	+	-	-	-	NA
RP	17GFE005	293	-	+	-	+	-	-
RP	17GFE154	295	+	+	-	-	-	-
RP	15ESE034	307	+	+	-	-	-	NA
RP	15ESE036	311	+	+	-	+	-	NA
RP	16GFE043	343	+	-	-	-	-	NA
RP	17GFE080	369	+	+	-	+	-	-
RP	17GFE137	369	+	-	-	+	-	-
RP	16GFE052	383	+	+	-	-	-	-
RP	16GFE056	393	-	-	-	-	-	-
RP	17GFE217	399	+	+	-	-	-	-
RP	17GFE124	413	+	-	+	-	-	-
RP	17GFE125	413	-	-	-	+	-	-
RP	17GFE126	413	-	-	-	-	-	-
RP	17GFE252	567	-	-	-	-	-	-
RP	17GFE255	598	-	-	-	+	-	-
		316,96	51,72%	34,44%	6,89%	27,58%	3,44%	***0%

*IPD: intrapulmonary dissemination; BL: bronchial lesions; AL: alveolar lesions; ADC: Adenocarcinoma.; NL: nasal lesions.

**Samples depicted in beige indicate mice that died prematurely due to other phenotypes (e.g. nasal tumor) and therefore did not live long enough to develop lung tumors with an expected longer latency such as SCLC. For this reason, we calculated two different penetrance, depicted as well in beige or in white, according to the considered mouse group.

***Nasal tumor are independent from lung tumors and have a much shorter latency, therefore their penetrance is calculated on the total mouse number.

Table S5. Neoplastic lesions developed by individual RP-Fgfr1 mice injected with Ad5-K14-Cre. Related to Figure 4.

K14	PROMAS	DAYS	SCLC	*IPD	*BL	*AL	*ADC	*NL
RP-Fgfr1	17GFE166	**88	-	-	-	-	-	+
RP-Fgfr1	17GFE171	102	-	-	-	-	-	+
RP-Fgfr1	17GFE188	130	-	-	-	-	-	+
RP-Fgfr1	17GFE191	138	-	-	-	-	-	+
RP-Fgfr1	17GFE202	160	-	-	-	-	-	+
RP-Fgfr1	17GFE216	172	+	+	-	+	-	-
RP-Fgfr1	17GFE224	197	-	-	-	-	-	+
RP-Fgfr1	17GFE225	207	-	-	+	-	+	-
RP-Fgfr1	17GFE283	252	+	+	-	-	-	-
RP-Fgfr1	18GFE003	281	-	-	-	-	-	-
RP-Fgfr1	18GFE008	291	-	-	-	+	-	+
RP-Fgfr1	18GFE049	340	+	+	+	+	+	+
RP-Fgfr1	18GFE055	351	+	+	-	+	+	+
RP-Fgfr1	18GFE060	357	+	+	+	+	-	-
RP-Fgfr1	18GFE070	370	+	+	-	+	+	NA
RP-Fgfr1	18GFE127	466	-	-	-	+	-	NA
RP-Fgfr1	18GFE051	344	-	-	+	-	+	+
		123,6	0%	0%	0%	0%	0%	***66,66%
		302,33	50%	50%	33,33%	58,33%	41,66%	

*IPD: intrapulmonary dissemination; BL: bronchial lesions; AL: alveolar lesions; ADC: Adenocarcinoma.; NL: nasal lesions.

**Samples depicted in beige indicate mice that died prematurely due to other phenotypes (e.g. nasal tumor) and therefore did not live long enough to develop lung tumors with an expected longer latency such as SCLC. For this reason, we calculated two different penetrance, depicted as well in beige or in white, according to the considered mouse group.

***Nasal tumor are independent from lung tumors and have a much shorter latency, therefore their penetrance is calculated on the total mouse number.

Table S6. Neoplastic lesions developed by individual RP mice injected with Ad5-K14-Cre. Related to Figure 4.

K14	PROMAS	DAYS	SCLC	*IPD	*BL	*AL	*ADC	*NL
RP	17GFE197	**111	-	-	-	-	-	+
RP	17GFE289	253	-	-	-	-	-	-
RP	17GFE328	267	+	+	-	-	-	-
RP	18GFE004	246	-	-	-	-	-	-
RP	18GFE006	251	+	+	-	-	-	-
RP	18GFE045	321	+	+	-	-	-	+
RP	18GFE056	320	+	+	-	+	-	-
RP	18GFE066	334	+	+	+	-	-	NA
RP	18GFE073	340	+	+	-	+	-	NA
RP	18GFE103	414	+	+	-	-	-	NA
RP	18GFE108	435	+	+	-	-	-	NA
RP	18GFE122	459	+	+	-	-	-	NA
RP	18GFE123	466	-	-	-	+	-	NA
RP	18GFE124	466	-	-	-	-	-	NA
RP	18GFE125	431	-	-	-	-	-	NA
RP	18GFE126	431	-	-	-	-	-	NA
			0%	0%	0%	0%	0%	***28,50%
		362,27	60%	60%	6,67%	20%	0%	

*IPD: intrapulmonary dissemination; BL: bronchial lesions; AL: alveolar lesions; ADC: Adenocarcinoma.; NL: nasal lesions.

**Samples depicted in beige indicate mice that died prematurely due to other phenotypes (e.g. nasal tumor) and therefore did not live long enough to develop lung tumors with an expected longer latency such as SCLC. For this reason, we calculated two different penetrance, depicted as well in beige or in white, according to the considered mouse group.

***Nasal tumor are independent from lung tumors and have a much shorter latency, therefore their penetrance is calculated on the total mouse number.

Table S7. Neoplastic lesions developed by individual RP-Fgfr1 mice injected with Ad5-SPC-Cre. Related to Figure 5.

SPC	PROMAS	DAYS	SCLC	*IPD	*BL	*AL	*ADC	*NL
RP-Fgfr1	16GFE093	125	-	-	-	-	+	+
RP-Fgfr1	17GFE003	142	-	-	-	-	+	-
RP-Fgfr1	16GFE114	144	-	-	-	-	+	-
RP-Fgfr1	16GFE082	147	-	-	-	-	+	-
RP-Fgfr1	16GFE084	150	-	-	-	-	+	-
RP-Fgfr1	16GFE085	151	-	-	-	-	+	-
RP-Fgfr1	16GFE090	151	-	-	-	-	+	-
RP-Fgfr1	16GFE091	151	-	-	+	-	+	-
RP-Fgfr1	16GFE119	153	-	-	-	-	+	NA
RP-Fgfr1	16GFE120	153	-	-	-	-	+	NA
RP-Fgfr1	16GFE099	162	-	-	-	-	+	NA
RP-Fgfr1	17GFE026	168	-	-	-	-	+	-
RP-Fgfr1	16GFE121	173	-	-	-	-	+	NA
RP-Fgfr1	16GFE118	182	-	-	-	-	+	NA
RP-Fgfr1	16GFE129	200	-	-	-	-	+	-
RP-Fgfr1	17GFE057	203	-	-	-	-	+	-
RP-Fgfr1	16GFE153	239	-	-	-	-	+	-
		164,35	0%	0%	5,88%	0%	100%	8,33%

*Besides SCLC, NE neoplastic lesions include IPD: intrapulmonary dissemination, BL: bronchial lesions; AL: alveolar lesions. ADC: Adenocarcinoma. NL: nasal lesions.

Table S8. Neoplastic lesions developed by individual RP mice injected with Ad5-SPC-Cre. Related to Figure 5.

SPC	PROMAS	DAYS	SCLC	*IPD	*BL	*AL	*ADC	*NL
RP	16GFE107	169	-	-	-	-	-	NA
RP	16GFE108	169	-	-	-	-	-	NA
RP	16GFE111	169	-	-	-	-	-	NA
RP	17GFE070	301	+	+	-	-	-	-
RP	17GFE153	417	-	-	-	-	-	-
RP	17GFE181	333	+	+	-	-	-	+
RP	17GFE187	357	+	+	-	-	-	-
RP	17GFE221	505	+	+	-	-	-	-
RP	17GFE226	434	+	+	-	-	-	-
RP	17GFE260	472	-	-	-	+	-	-
		332,6	50%	50%	0%	10%	0%	14,29%

*Besides SCLC, NE neoplastic lesions include IPD: intrapulmonary dissemination, BL: bronchial lesions; AL: alveolar lesions. ADC: Adenocarcinoma. NL: nasal lesions.

Table S9. Neoplastic lesions developed by individual RP-Fgfr1 mice injected with Ad5-CC10-Cre. Related to Figure 5.

CC10	PROMAS	DAYS	SCLC	*IPD	*BL	*AL	*ADC	*NL
RP-Fgfr1	17GFE030	253	-	-	-	-	+	NA
RP-Fgfr1	17GFE031	253	-	-	-	-	+	NA
RP-Fgfr1	17GFE032	253	-	-	-	-	-	NA
RP-Fgfr1	17GFE043	268	-	-	-	-	+	-
RP-Fgfr1	17GFE059	279	-	-	-	-	+	-
RP-Fgfr1	17GFE072	290	-	-	-	-	+	-
RP-Fgfr1	17GFE088	310	-	-	-	-	+	-
RP-Fgfr1	17GFE115	330	-	-	-	-	+	-
RP-Fgfr1	17GFE167	399	-	-	-	-	+	+
		292,78	0%	0%	0%	0%	88,89%	16,67%

*Besides SCLC, NE neoplastic lesions include IPD: intrapulmonary dissemination, BL: bronchial lesions; AL: alveolar lesions. ADC: Adenocarcinoma. NL: nasal lesions.

Table S10. Neoplastic lesions developed by individual RP mice injected with Ad5-CC10-Cre. Related to Figure 5.

CC10	PROMAS	DAYS	SCLC	*IPD	*BL	*AL	*ADC	*NL
RP	16GFE146	184	-	-	-	-	-	-
RP	17GFE033	253	-	-	-	-	-	NA
RP	17GFE034	253	-	-	-	-	-	NA
RP	17GFE035	253	-	-	-	-	-	NA
RP	17GFE150	370	+	+	-	-	-	-
RP	17GFE156	380	-	-	-	-	-	-
RP	17GFE247	549	+	-	-	+	-	-
RP	17GFE253	555	-	-	+	-	-	-
RP	17GFE259	555	+	-	-	+	-	-
RP	17GFE262	555	-	-	-	-	-	-
		372,44	30%	10%	10%	20%	0%	0%

*Besides SCLC, NE neoplastic lesions include IPD: intrapulmonary dissemination, BL: bronchial lesions; AL: alveolar lesions. ADC: Adenocarcinoma. NL: nasal lesions.

Table S11. Penetrance of lung lesions according to the targeted cell-of-origin and genotype. Related to Figure 1, 4, 5.

VIRUS	GENOTYPE	MICE #	SCLC	*IPD	*BL	*AL	*ADC	*NL
CMV	RP	22	90%	90%	55%	50%	0%	15%
	RP-Fgfr1	10	20%	0%	80%	70%	80%	64%
CGRP	RP	29	52%	34%	7%	28%	3%	0%
	RP-Fgfr1	17	18%	18%	29%	35%	41%	70%
K14	RP	15	60%	60%	7%	20%	0%	29%
	RP-Fgfr1	12	50%	50%	33%	58%	42%	67%
SPC	RP	10	50%	50%	0%	10%	0%	14%
	RP-Fgfr1	17	**0%	**0%	6%	0%	100%	8%
CC10	RP	10	30%	10%	10%	20%	0%	0%
	RP-Fgfr1	9	**0%	**0%	0%	0%	89%	17%

*IPD: intrapulmonary dissemination; BL: bronchial lesions; AL: alveolar lesions; ADC: Adenocarcinoma.; NL: nasal lesions

** RP-Fgfr1 mice were sacrificed earlier than RP mice, due to the presence of huge lesion of LADC; therefore we cannot exclude a late appearance of SCLC.

Table S12. Latency range of lung tumors in RP mice injected in this study compared to previous publication by Sutherland et al., 2011. Related to Figure 5

Virus	Latency Range	Study
CGRP	268-413	Ferone et al., 2020
CGRP	255-464	Sutherland et al., 2011
SPC	301-505	Ferone et al., 2020
SPC	319-616	Sutherland et al., 2011
CC10	370-555	Ferone et al., 2020
CC10	389-640	Sutherland et al., 2011

Table S13. Comparison across a variety of studies of tumor type and location obtained in *Trp53$^{F/F}$;Rb1$^{F/F}$* mouse models by targeting distinct cell types. Related to Figure 7

Target cells	Genetics	Inducer	Tumor type and location	Reference
NE	*Trp53$^{F/F}$;Rb1$^{F/F}$*	*IT Ad5-CGRP-Cre	SCLC in central lung	Sutherland et al., 2011
CLUB	*Trp53$^{F/F}$;Rb1$^{F/F}$*	IT Ad5-CC10-Cre	Rare ADC in alveolar space	Sutherland et al., 2011
AT2	*Trp53$^{F/F}$;Rb1$^{F/F}$*	IT Ad5-SPC-Cre	SCLC in central lung	Sutherland et al., 2011
All lung	*Trp53$^{F/F}$;Rb1$^{F/F}$*	IN Ad-Cre	SCLC in main airways; *BADJs	Park et al., 2011
CLUB	*Trp53$^{F/F}$;Rb1$^{F/F}$; Scgb1a1-Cre*	constitutive	No tumors	Park et al., 2011
AT2	*Trp53$^{F/F}$;Rb1$^{F/F}$*	*IN Ad-SPC-CreER + *Tam	Rare ADC in alveolar space	Park et al., 2011
AT2	*Trp53$^{F/F}$;Rb1$^{F/F}$;p130$^{F/F}$*	IN Ad-SPC-CreER + Tam	Rare ADC in alveolar space	Park et al., 2011
AT2 and bronchial cells	*Trp53$^{F/F}$;Rb1$^{F/F}$; SPC-rtTA/(tetO)7-Cre*	*Dox	Rare ADC in alveolar space (also without induction by Dox)	Park et al., 2011
All lung cells	*Trp53$^{F/F}$;Rb1$^{F/F}$;p130$^{F/F}$*	IT Ad5-CMV-Cre	SCLC in proximal and distal airways and BADJ	Yang et al., 2018
NE	*Trp53$^{F/F}$;Rb1$^{F/F}$;p130$^{F/F}$*	IT Ad5-CGRP-Cre	Fewer SCLC in proximal airways	Yang et al., 2018

*IT = intratracheal delivery; IN = intranasal delivery; BADJs = bronchioalveolar duct junctions; Tam = Tamoxifen; Dox = Doxycycline